JUSTUS-LIEBIG-
UNIVERSITÄT
GIESSEN

BESIII

Master Thesis

Analysis of the decay $e^+e^- \to \gamma X(3872) \to J/\psi\gamma\gamma$ at the BESIII experiment

Analyse des Zerfallskanals $e^+e^- \to \gamma X(3872) \to J/\psi\gamma\gamma$ am BESIII Experiment

Svende Annelies Braun

März 2014

Justus-Liebig-Universität Gießen
II. Physikalisches Institut

Advisor:
Prof. Dr. Wolfgang Kühn
Dr. Jens Sören Lange (AR)

Abstract

In the charmonium region many states have been observed which are not predicted by theoretical models, such as the $X(3872)$ state that can not be conventional charmonium. Since the nature of these exotic states still remains unknown, a search is performed for the process $e^+e^- \to \gamma X(3872)$ and the subsequent decay of $X(3872) \to J/\psi\gamma$. This study is done with data samples collected with the BESIII detector operating at the symmetric BEPCII storage ring in Beijing, China at center-of-mass energies, right at the exotic $Y(4260)$ and $Y(4360)$ resonances. The statistical significance for this process is calculated to be 1.59 σ for the sum of all data samples, which is far away from a real observation. Upper limits for the product of cross section $\sigma[e^+e^- \to \gamma X(3872)]$ and branching fraction $\mathcal{B}(X(3872) \to J/\psi\gamma)$ have been calculated to be smaller than 0.617 pb, 1.061 pb and 0.493 pb at center-of-mass energies of 4.229 GeV, 4.260 GeV, and 4.360 GeV at 90 % confidence level.

Contents

In this thesis all equations are presented in natural units

$$\hbar = c = 1$$

as common in the field of high energy physics. This means that all masses, energies and momenta are measured in the same unit in powers of eV (MeV, GeV).

1 Introduction

The Beijing Electron Spectrometer III (BESIII) experiment is located at the Beijing Electron-Positron Collider II (BEPCII) in Beijing, China at the Institute for High Energy Physics (IHEP) to study symmetric e^+e^- collisions up to a maximum center of mass energy of 4.66 GeV and to do precision measurements on light hadron, τ physics and charmonium spectroscopy. So far it has accumulated the world largest data set of J/ψ, $\psi(2S)$, $\psi(3770)$ and $\psi(4040)$ events in e^+e^- collisions and offers so unique opportunities to study those states.

In this mass region recently many new states which do not fit into the charmonium spectrum have been observed by various experiments. These states were called XYZ states, where X corresponds to unknown states, Y to vector states like $Y(4260)$, $Y(4360)$ and Z to charged charmonium-like states. Due to their special properties they are believed to be QCD allowed exotic states rather than conventional charmonium.

In 2003 the Belle Collaboration found an unexpected narrow state above the $D\bar{D}$ threshold, which they called $X(3872)$. Due to its mass close to the $D\bar{D}^*$ threshold and its isospin violating decays it is a good candidate for a hadronic molecule or tetraquark.
Since then the $X(3872)$ was only observed in B meson decays and hadron collisions. BESIII recently observed the decay of $X(3872) \to J/\psi\pi^+\pi^-$ in $e^+e^- \to \gamma X(3872)$ in the charm system for the first time as well as other charged unconventional states containing charm and anti-charm quarks.
The nature of these exotic states still remains unknown. To further understand their nature searches for other decay processes are necessary.

In this thesis a search for radiative transitions of $Y(4260)$ and $Y(4360)$ to the lower lying charmonium-like $X(3872)$ state is performed, where the $X(3872)$ is reconstructed through $J/\psi\gamma$. Such investigations should help to clarify the existence of the radiative decay of $Y(4260) \to \gamma X(3872)$ as studied with a different final $J/\psi\pi^+\pi^-$ state by BESIII [1].

2 Theoretical Background

2.1 The Standard Model

The goal of particle physics is to understand our universe at the level of its fundamental constituents of matter, the elementary particles which as far as we know are quarks and leptons. The Standard Model (SM) of particle physics is the theoretical framework, putting together all elementary particles and their fundamental interactions, excluding gravity.

Quarks and Leptons are the **elementary matter particles** of the SM, with a half integer spin, called fermions. To our current knowledge they do not posses substructure and can therefore not be excited. Quarks and leptons can be further divided into three so-called generations, each containing a charged lepton and the corresponding neutral neutrino as well as a positively and a negatively charged quark. The generations differ only by their mass, they are summarized in Table 1.

Fermions	Generation			Electric	Color	Weak
	1	2	3	Charge	Charge	Charge
Leptons	ν_e	ν_μ	ν_τ	0	-	yes
	e	μ	τ	-1	-	yes
Quarks	u	c	t	$+2/3$	r, b, g	yes
	d	s	b	$-1/3$	r, b, g	yes

Table 1: Properties of Fermions in the Standard Model

It is still an open question why there are exactly three generations of fermions, but due to the precisely measured width of the Z^0 resonance the room for more is rather small since its excludes a forth fermion family below the Z mass. All stable matter is made of up and down quarks in form of protons and neutrons as well as electrons.

Interactions between the particles are mediated by the elementary force carriers called gauge bosons with integer spin.
The **electromagnetic interaction** is mediated via photons which couple to the electric charge of particles. The range of the interaction is infinite since the photon is massless and has no electric charge. It is described in terms of quantum electrodynamic (QED) and it is the most accurately tested elementary theory so far.

The **weak interaction** is mediated by the exchange of massive force carriers $W^\pm$ and Z^0 with masses of $m_W = 80.385 \pm 0.015$ GeV and $m_Z = 91.1876 \pm 0.0021$ GeV [2]. Quantum field theories (QFT) allow only massless gauge bosons due to the gauge symmetries. The gauge bosons gain masses through the mechanism of electroweak symmetry breaking (EWSB) of the Higgs field. The existence of the corresponding Higgs particle was experimentally confirmed by the observation of a Higgs-like Boson in 2012 at the LHC [3, 4], which led to the award of the Nobel Price in Physics 2013 for the theory of how particles acquire mass to François Englert and Peter W. Higgs.

The range of the weak interaction is short ($\sim 10^{-18}$ m) due to the heaviness of its gauge bosons. Therefore weak decays are much weaker because its field strength over a given distance is typically several orders of magnitude less than that of the other forces. This leads to the long lifetime (~ 15 min) for the free neutron, where the down quark decays weakly and changes its quark flavour into a up quark.
The weak interaction couples only to left-handed fermions and right-handed anti-fermions, there by violating parity maximally. It also violates the combined symmetry of parity and charge conjugation CP, which is a much smaller effect and therefore does not explain the asymmetry between matter and antimatter symmetry observed in nature.

The **strong interaction** is mediated by gluons as its gauge bosons. They are massless and couple to the color charge carried by quarks and gluons themselves. This self coupling makes the theory of strong interaction, called Quantum Chromo-Dynamics (QCD) so complicated and hard to calculable. The range of the strong interaction is limited to the scale of nucleon's ($\sim 10^{-15}$m) since only color-neutral objects have finite energy and neither quark or anti-quark exist as isolated particles and can be directly observed due to the *confinement*. The potential energy between two quarks rises until a new quark-antiquark pair is created out of the vacuum, as one tries to separate two quarks. The linear rising of the potential is explained by the gluon self interaction, leading to flux tube formation between interacting quarks. The gluonic self-interaction also leads to the running of the strong coupling constant α_s: if the distance between coloured objects is small, corresponding to high momentum scales, quarks behave as almost free particles with no interaction between them. This is known as the so-called *asymptotic freedom* of QCD where the coupling constant is small and pertubative QCD (pQCD) can be used to calculate different processes.
QCD allows all color-neutral combinations of quarks and gluons (hadrons) bound by the strong force: mesons (quark-antiquark), baryons (three quarks) and other more exotic combinations like multiquark states (tetra- or pentaquarks), hybrids with constituents $q\bar{q}g$ or glueballs (ggg). Meson-molecules which are built of two neutral mesons bound by color forces between its constituents would be also allowed. This is already common for Baryons since any nucleus with two (deuteron) or more baryons can be seen as a baryonic molecule. Exotica are of great interest for the understanding of QCD and a search for them is part of this thesis.

Gravitation acts on all particles with mass, but it is small compared to the other interactions. Therefore it is negligible at the scale of quarks and hadrons, but it is the dominating force at cosmic scales because its range is infinite and it is always attractive. This interaction is not included in the SM since there is no QFT theory available which describes the gravitational interaction yet. So far the best theoretical description is Einstein's classical theory of general relativity, which does not include quantum effects. Several different theories try to unify these interactions like theory of everything (TOE) which are far from being experimentally provable in energy ranges well beyond TeV where only the TeV range is so far reachable at the LHC.
Therefore the Standard Model is not complete and can not be the ultimate the-

ory of nature, since many questions are not solved such as the matter-antimatter asymmetry in the universe and neutrino oscillations implying a non-zero mass of the neutrino which is not included in the SM. For this reason many experiments search for Physics beyond the SM (BSM). On one side the LHC proves the highest possible energy region and high precision experiments such as BESIII,BELLE, BELLE II and LHCb are used to test for small deviations from predicted SM values up to very high precision.

2.1.1 Quantum Field Theory

The theoretical foundations of the SM can be phrased in the mathematical framework of QFT. One of its basic principles of the interactions realized in nature is local gauge invariance which describes the invariance of a symmetry under a change of local coordinates ,a shift or a rotation, that does not change the underlying physics. In this context group theory is used (unitary Lie groups) and the full symmetry of the SM can be written as

$$U(1) \times SU(2) \times SU(3) \tag{1}$$

which is the product of three symmetry groups: $U(1)$ is describing the symmetry of the electromagnetic interaction with the photon as the mediating gauge boson. $SU(2)$ describes the weak interaction which only acts on left-handed fermions. The number of its corresponding gauge bosons is given by $n = dim^2(group) - 1$, in this case three gauge bosons. These two interactions can be unified into the electro-weak force which is described by Yang-Mills theories. $SU(3)$ is the special unitary group of dimension three with eight gluons as gauge bosons describing the strong interaction. The corresponding colour charges are red(r), green(g) and blue(b) carried by quarks and gluons.
The idea of QFT is to describe the particles in terms of fields $\phi_i(x, y, z, t)$ and it consists of equations describing movement and interactions of fields. They can be described in terms of the Lagrange formalism, where instead of using a Lagrangian as a function of coordinates q_i as in classical mechanics, a Lagrangian density $\mathcal{L}$ is used which combines the relativistic dynamics and kinematics of the theory.

2.2 Symmetries and Conservation Laws

Noether's Theorem from 1917 directly relates symmetries and conservation laws [5]: Each symmetry of nature leads to a conservation law, and vice versa every conversation law reflects an underlying symmetry. Symmetry reflects an operation on a system that leaves it invariant.
All physics processes (e.g. the production and the decay of particles) need to conserve energy, momentum and angular momentum. Those are general conservation laws and are related to translations in time, space and invariance under rotations. From special relativity the energy-momentum relation $E^2 = m^2 + \vec{p}^2$ is known which leads to the invariant mass of particles $\sqrt{s} = m = \sqrt{E^2 - \vec{p}^2}$. The invariance of this quantity with respect to different reference systems is necessary since it is used to reconstruct intermediate particles from their decay products.

Dynamical conservation laws include electric charge (invariance of electrodynamics under gauge transformations), colour, baryon number (+1 for baryons, -1 for antibaryons and 1/3 for quarks) and lepton number conservation. Quark flavour (u,d,s,c,b,t) is conserved in the electromagnetic and strong interaction, but not in weak interactions.

Discrete symmetries include parity, charge conjugation and time reversal. Parity describes a mirror symmetry around the origin and acts on the wave function of a system: $\hat{P}\,|\psi(r)\rangle = P\,|\psi(r)\rangle$ where P can have eigenvalues ± 1. The charge conjugation operator changes particles into antiparticles $\hat{C}\,|\psi\rangle = C\,|\bar{\psi}\rangle$ with C=$\pm$1. Only particles that are their own antiparticles can be eigenstates of C. The Time reversal operator $\hat{T}$ changes the wave function in time. This value is believed to be violated in the EW theory due to CP violation of the weak interaction since the combined operation is an exact symmetry of any interaction, which is included in the TCP theorem as an result of QFT [5].

2.3 Quarkonium

Heavy quarkonium refers to states which are built of heavy quarks (compared to the mass of the lighter quarks u, d and s): c and $\bar{c}$ (charmonium) and b and $\bar{b}$ (bottomonium) quarks. States made of t and $\bar{t}$ quarks (topmonium) do not exist since these are so massive that they decay via the weak interaction before they can hadronize.

Bound systems formed by the electromagnetic interaction (QED), namely positronium can be used as an analogy to describe heavy quarkornia in QCD. **Positronium** is a bound system of e^+e^- that is close to the quarkonium system due to the same mass of its constituents that leads to a small binding energy. Furthermore the system has a finite lifetime due to annihilation processes into two or three photons. This system has many different energy levels which can be calculated by solving the non-relativistic Schrödinger-equation to $E_n = -\frac{\alpha^2 mc^2}{4n^2}$ without fine and hyperfine splitting corrections. Here the various energy levels are relatively close to each other with a spacing of several electron volts, which is only a small fraction of the total rest energy of the system. Therefore all states are seen as a part of the positronium with a very small lifetime [5]. In QED the coupling strength and the corresponding potential are very well known since the force is electromagnetic. All possible transitions, energy levels and lifetimes can be calculated and agree very well with experimental measurements.

In **quarkonium** on the other hand quark and antiquarks can also form a bound system, but here the energy spacings between different states of the bound quark system are very large compared to their width, so that we regard them as distinct particles which do not overlap and give the different excited states of the same bound quark system their own names. The nomenclature for this is given by $n^{2S+1}L_J$, where $n_{q\bar{q}} = N + 1$ with N as the number of knots in the radiative part R of the wave function of the system, if it can be separated by the product ansatz into $\Psi(r, \theta, \phi) = R_{kl}(r) \cdot Y_l^m(\theta, \phi)$. L is the orbital angular momentum and determines

the orbit of the system (S,P,D,F,...). It can be combined with the total spin S to the total angular momentum J by $|L - S| \leq J \leq L + S$. A more common notation is J^{PC}, where P is the parity quantum number of the system given by $P = (-1)^{L+1}$ and C the charge conjugation $C = (-1)^{L+S}$.

Unlike hydrogen and positronium, the quarks in heavy quarkonium are bound by the strong force so the question is what potential to use instead of Coulomb's law or how to incorporate magnetism to obtain the spin couplings [5]. In principle QCD determines all meson properties like masses, widths and decay rates, but the strong-interacting quarkonium systems are not calculable from first principles in QCD continuously due to their lower energy region, where the running coupling constant α_s is too big to apply perturbation theory. Lattice QCD is a method from first principles which calculates the quantities at discrete lattice spacings, but so far it was not possible to calculate the whole charmonium spectrum. Therefore models are needed to describe the potential, some of them even use experimental results from transition measurements, cross sections and branching ratios as an input for their phenomenological models so that collaboration between theory and experimentalists is needed to improve the knowledge about the bound system. Non-relativistic approximations such as effective field theories and lattice calculations can be used to describe quarkonium spectra since the quark masses are the dominating contribution to the heavy quarkonia masses. The precise measurement of the spectra and the comparison to the predictions from theory are crucial for the understanding of QCD, since they can be used to probe the low energy non-perturbative region of QCD and to put it on its stringent tests.

2.3.1 The QCD potential

A simple phenomenological model, the Cornell potential [6], can be used to calculate the energy levels of the different states which is based on similarities of chromodynamics to electrodynamics at short distances. Here the behaviour is dominated by the one-gluon exchange just as QED is dominated by the Coulomb-like one-photon exchange. Since both mediating particles are massless, the interactions are identical apart from the coupling strength α_s and color factors $(\frac{4}{3})$ which come from counting the number of gluons contributing to a given process. This only works for short distances. At large distances one has to take into account the quark confinement this means that the potential increases without a limit. In this model this is done by adding a linear potential corresponding to a constant force with the string tension k which reflects the confinement:

$$V(r) = -\frac{4}{3}\frac{\alpha_s}{r} + kr. \tag{2}$$

A more sophisticated approach is to include more additional interactions like spin-spin, spin-orbit and magnetic dipole interactions arising from the two quarks which

leads to spin-tensor terms as done in [7]. This leads to the potential

$$\begin{aligned} V(r) = & - \frac{4\alpha_s}{3r} + k \cdot r + \frac{4\pi\alpha_s}{3m_c^2}\delta(\vec{r}) + \frac{2\alpha_s}{3m_c^2}\left[\frac{\vec{p}\cdot\vec{p}}{r} + \frac{(\vec{r}\cdot\vec{p})(\vec{r}\cdot\vec{p})}{r^3}\right] \\ & + \frac{4\pi\alpha_s}{3m_c^2}\left[\frac{8\pi}{3}\delta(\vec{r})(\vec{s}_c\cdot\vec{s}_{\bar{c}}) + \frac{3(\vec{s}_c\vec{r})\cdot(\vec{s}_{\bar{c}}\vec{r}) - \vec{s}_c\cdot\vec{s}_{\bar{c}}}{r^3}\right] \\ & + \frac{2\alpha_s}{m_c^2}\frac{(\vec{r}\times\vec{p})\cdot(\vec{s}_c+\vec{s}_{\bar{c}})}{r^3} \end{aligned} \tag{3}$$

based on a one-gluon exchange. Here m_c is the mass of the charm quark, $\delta(\vec{r})$ the Dirac delta function, $\vec{p}$ and $\vec{r}$ are the momentum and spatial coordinates and $\vec{s}$ is the spin of the quark. A linear confinement term is derived from lattice QCD calculations for the limit of static quarks. With this potential the spectra can be calculated by solving the non-relativistic radial Schrödinger equation.

2.3.2 The Charmonium Spectrum

Figure 1 [8] shows an overview the calculated charmonium spectra, the experimentally observed states as well as some seen transitions between those states for all different possible quantum numbers J^{PC}. Here the strong coupling constant α_s is fixed to 0.29, the mass of the charm quark approximated by 1.22 GeV and the string tension k to 1.3 GeV. The first two values are set to reasonable values as discussed in [2], whereas the latter one is about 30% larger than results from lattice QCD calculations [7].
The calculated spectra from equation (3) are indicated as red squares and the measured states as lines. From the spectrum one can see that for states below the $D\bar{D}$ threshold the calculated states fit the observed states rather well, but for states close to or above the open charm threshold there are huge differences. In this regions the model cannot reproduce the spectrum, for example vector charmonium states are predicted much too high. The model also predicts charmonium states which have not been observed so far as the h_c' and higher excited χ_c'.

States which are marked in black are understood as conventional charmonia made off $c\bar{c}$ since their masses and widths can be predicted by more advanced models calculated in [9]. States below the $D\bar{D}$ threshold can only decay via a strong decay with three virtual gluons produced as a virtual state which has to have enough energy to produce $q\bar{q}$ as shown in Figure 2. These decays below the open charm threshold are called OZI suppressed decays since their mass is too small to decay into open charm final states. This is the reason why these states are relatively long-lived ($\sim 10^{-20}$ s) with a narrow width of about 100 keV compared to states made off u,d and s quarks with much smaller lifetimes. Those light quark states are therefore broad so that they mix with each other and can not be clearly separated which makes them experimentally much harder to observe. This feature makes heavy quarkonium spectroscopy so interesting and also easier to study.
States above the $D\bar{D}$ threshold decay OZI allowed into two charmed D mesons as shown in Figure 2 on the right, which results in a much shorter lifetime. Those

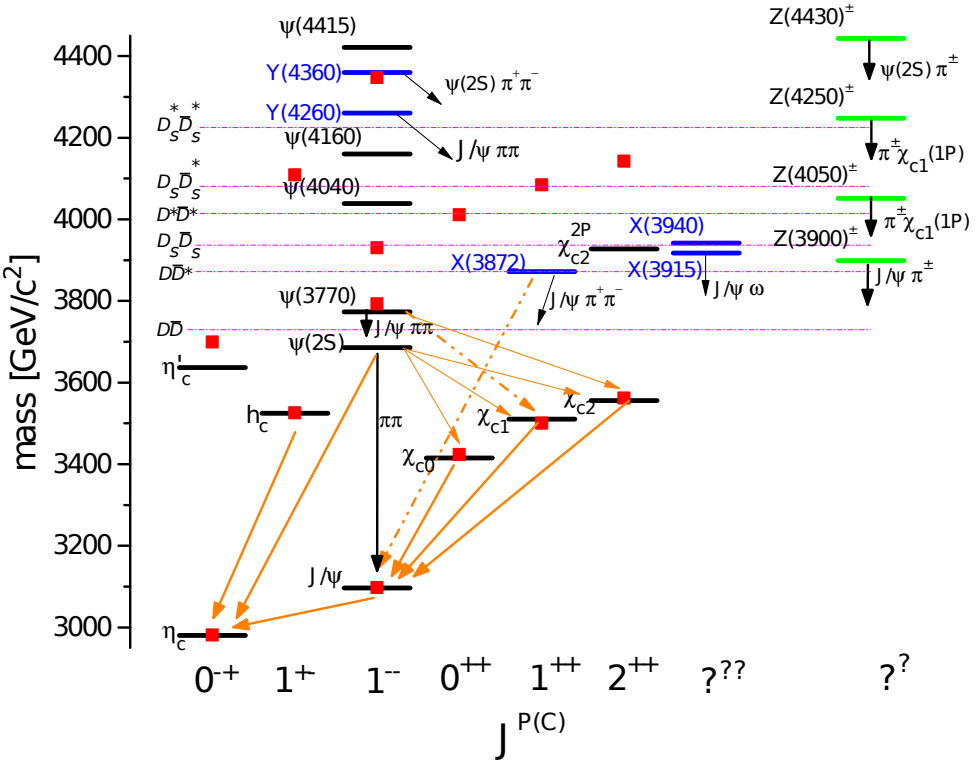

Figure 1: The measured charmonium spectrum [8] compared to model calculations from equation (3) which are shown as red squares. The model also predicts states which haven't been observed yet. The black lines indicate experimental measured states, which are believed to be conventional charmonium states. The blue lines mark observed states which do not fit into the spectrum. The arrows show some observed transitions between the charmonium states, the orange ones indicate radiative photon transitions, whereas opening $D\bar{D}$ thresholds are drawn in purple. The green lines describe measured charged resonances (Z) which are clearly not only made off $c\bar{c}$ due to their charge but a more exotic combination. Those charged states don't belong to the charmonium spectrum, there are included here because they were observed in transitions into charmonia as indicated by the black errors.

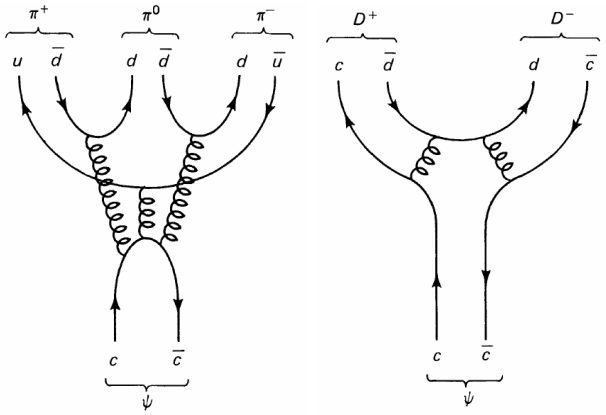

Figure 2: Decays of charmonium, left shows OZI supressed decay for charmonium below the $D\bar{D}$ threshold and right shows OZI allowed decays for charmonium above the $D\bar{D}$ threshold [5]

states have a larger width of several MeV.

States which are marked in blue are experimentally measured states observed by different experiments like the X and Y states, which do not seem to fit into the charmonium spectrum. Either their measured properties like mass and width are inconsistent with predicted conventional charmonium or their quantum numbers are not measured yet as for the $X(3940)$. They gained a lot of attention when they were discovered for the first time because they are believed to be good candidates for an exotic QCD allowed form of matter like hybrids, glueballs or tetraquarks. The question if such states are existing is one of the important issues which might be answered by heavy quarkonium spectroscopy in the near future.

This thesis is focused on the $X(3872)$ state which was the first observed exotic candidate, its special properties are further explained in the next section.

All green marked Z states are charged-charmonium like states which have been recently discovered and confirmed by various experiments [10–15]. They can not be conventional $c\bar{c}$ due to their charge and must consist of at least of four quarks. They have been observed in decays into charmonium and charged pions and some of their transitions are indicated by the black arrows, but also more final states have been published recently [16, 17]. Their nature is widely discussed in the physics community at the moment.

2.4 The $X(3872)$ state

The charmonium system and its fundamental role in the development of QCD was thought to be rather well understood since most of the states below the open charm threshold were discovered and well described with models employing QCD inspired potentials. Charmonium spectroscopy gained a lot of new attention with the discovery of the charmonium-like $X(3872)$ state by BELLE in 2003 in the decay channel $B^{\pm} \to K^{\pm}X(3872) \to K^{\pm}J\psi\pi^{+}\pi^{-}$ [18], which was confirmed by several other experiments ([19],[20],[21]). Since its discovery the state has stimulated special interest for its nature and has a special role in the list of unanticipated states since its the first observed and the most intriguing one [22]. In the last ten years it has been widely studied but its interpretation demands much more experimental investigations. Its apparent quantum numbers, mass, and decay patterns make it an unlikely to be a conventional charmonium candidate, and so far no consensus explanation has been found to explain all measured properties.

The same final state $X(3872) \to J\psi\pi^{+}\pi^{-}$ was also studied by CDF [23] in terms of angular distributions and correlations in the $\pi^{+}\pi^{-}$ system and found that the dipion system was dominated by a $\rho^{0}(770)$ resonance, which would mean an isospin of one in the final state. Their measurements could only be explained by a quantum number assignment of $J^{PC}(X(3872)) = 1^{++}$ or 2^{-+}. Both *BABAR* and Belle have observed $X(3872) \to J/\psi\gamma$ decays ([24],[25]), this radiative decay verifies the positive C-parity assignment of CDF. Even more: a $J^{PC} = 2^{-+}$ state would have to

undergo a higher-order multipole transition to decay into $J/\psi\gamma$ which would be more suppressed than the observed rates allow [22]. Finally, LHCb did a measurement of the quantum numbers by analysing the angular distribution of $X(3872)$ in B meson decays [26]. Their data favours 1^{++} over the 2^{-+} hypothesis at a significance of 8.4σ.

Since its discovery the proximity of the $X(3872)$ mass to $D^{*0}\bar{D}^0$ threshold was conspicuous, and even decays to $D^{*0}\bar{D}^0$ were observed by *BABAR* [27] and Belle [28] with branching fractions about ten times higher than into $J\psi\pi^+\pi^-$ final state. Because of this relation, precise mass measurements of the $X(3872)$ mass as well as the D mass have been done. The world average mass of the $X(3872)$ is given by 3871.68 ± 0.17 MeV, together with the D^0 mass measurement this leads to a difference of $m[X(3872)] - [m(D^{0*}) + m(\bar{D}^0)] = -0.17 \pm 0.26$ MeV [2]. This and other properties led to various speculations about the nature of the $X(3872)$ which are further discussed in the next section.

Moreover Belle found a 4.3 σ evidence for the decay $X(3872) \to J/\psi\pi^0\pi^+\pi^-$ where the pions come from the ω low-side tail resonance[29]. The rate in $J/\psi\omega$ was found to be comparable to $J\psi\pi^+\pi^-$. This was confirmed by *BABAR* in 2010 with a significance of 4.0 σ [30]. These roughly equal rates are one of the most interesting properties of the $X(3872)$ because it means that it decays into final states with isospin one (of the ρ^0) and isospin zero (of the ω) with the same strength.

BABAR also found evidence for the radiative decay into $\psi(2S)\gamma$ [31] with a rate of $\frac{\Gamma(X(3872)\to\psi(2S)\gamma)}{\Gamma(X(3872)\to J/\psi\gamma)} = 3.4 \pm 1.4$ which has not been seen by Belle [25] so they give an upper limit which is inconsistent with the *BABAR* result.
Searches for charged partners of the $X(3872)$ in the decay $X(3872) \to J/\psi\rho^+$ have been done by *BABAR* [32] which gave the conclusion that $X(3872)$ is most likely an isosinglet.

The width of the state was measured to be very small with an upper limit of $\Gamma < 1.2$ MeV at 90% C.L.[2]. Compared to conventional charmonium above the $D\bar{D}$ which decay OZI allowed this differs by more than one order of magnitude and is the most intriguing fact making the $X(3872)$ an exotic candidate.

2.5 Possible $X(3872)$ interpretations

The $X(3872)$ was the first observed state of the now so-called XYZ family. Since then many more charmonium and bottomonium-like states have been reported in experiments with different production mechanisms: initial state radiation(ISR), double charmonium production, two photon fusion, B-decays and excited charmonium or bottomonium decays compared to Figure 3. These observations led to extensive discussions about the underlying nature of these states. Theoretical speculations include di-meson molecular states, tetraquarks, hybrid charmonium and conventional charmonium. Because many of these new states lie very close to different open-charm thresholds, ideas were investigated that those measurements are threshold

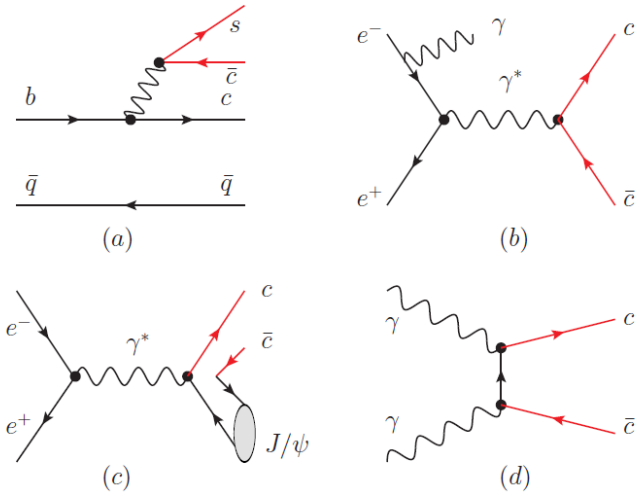

Figure 3: Feyman diagrams for the production mechanism of XYZ states from [33]. a) describes B meson decays ($B \to K + XYZ$), b) shows ISR e^+e^- annihilation ($e^+e^-(\gamma_{ISR}) \to XYZ$) , c) for double charm production ($e^+e^- \to J/\psi XYZ$) and d) gives the $\gamma\gamma$ fusion process($\gamma\gamma \to XYZ$)

enhancement effects rather then real resonances as cusp effects, final state interactions or interferences between continuum and well-known charmonium states.

The first idea was that the $X(3872)$ is the missing excited conventional charmonium state $\chi(2S)_{c1}$ since it has the same quantum numbers, but the mass is about 50 MeV away from the χ'_{c1} mass predicted in [9]. Also, as mentioned before, the width is too small for a conventional charmonium above the $D\bar{D}$ threshold. Other than being χ_{c1} the $X(3872)$ could still be conventional charmonium since the quark model spectrum can be distorted by coupled-channel and screening effects so that the energy level spacing becomes narrower above 4 GeV. (See [34] for more information.)

Among all theoretical proposals about the $X(3872)$ nature, the molecular state is the most popular because of the mass proximity to the $D^{*0}\bar{D}^0$ threshold. Molecular states are thought to be loosely bound states of two heavy mesons, in this case a superposition of $D^{*0}\bar{D}^0$ and $\bar{D}^{*0}D$. Due to the tiny binding energy and separations of D^{*0} and $\bar{D}^0$ of several fermi they would be bound by long range pion exchange what can be calculated with chiral effective field theory(χEFT). This model would also explain the decay into the isospin violating mode $J/\psi\rho$ [33]. So far prediction from the molecular picture are in contradiction to the measured branching ratios of different decay modes, as discussed in [33]. This feature is still discussed controversially by different groups of theorists, but it would be far too early to rule out this possibility of being a molecule.

Another idea for its nature is to be a tetraquark, which are four quarks bound by the coloured force between quarks. These states do decay through rearrangement of the quarks. In this picture there should be many states within the same tetraquark multiplet which are charged or carry stangeness [9]. The tightly bound

diquark-diantiquark system ($cu\bar{c}\bar{u}$) should have the neutral partners ($cd\bar{c}\bar{d}$,$cd\bar{c}\bar{s}$) and one charged partner ($cu\bar{c}\bar{d}$). However this interpretation is limited by the non-observation measurement for the charged partner made by *BABAR* [32].

Moreover it is possible that the $X(3872)$ is a QCD allowed hybrid exotic state. Hybrid charmonium states are bound states built of a valence quark-antiquark and one additional gluon which carries an additional degree of freedom.

2.6 The $Y(4260)$ and $Y(4360)$ state

Another puzzling state is the $Y(4260)$ which was observed as an unexpected vector charmonium-like state in ISR production of $Y(4260) \to \pi^+\pi^- J/\psi$ by *BABAR* [35] and confirmed by several other experiments [36, 37]. One more excited vector enhancement $Y(4360) \to \pi^+\pi^-\psi(2S)$ was found by *BABAR* [38] and confirmed by Belle [39]. Because the dipion transition between vector quarkonia is quite common for charmonium and bottomonium, those were first ascribed to be excited vector charmonia (Y), because of their ISR production through a virtual photon.
The issue is that there are no predicted 1^{--} states close to those masses and the width of ≤ 100 MeV is quite narrow for states far above the $D\bar{D}$ threshold. Moreover both states do not show up in the inclusive hadron cross section (R-scan) measurement as would be expected of such states [22]. It is also interesting that the decay width $\Gamma(Y \to \pi^+\pi^- J/\psi)$ is an order of magnitude higher than expected for conventional vector charmonium states, since charmonium would dominantly decay into open charm final states, exceeding the dipion transition by a factor ≤ 100 as it has been measured for $\psi(3770)$ [22]. So far the only other seen decay mode is $\pi^0\pi^0 J/\psi$ measured by CLOE with half the rate of the decay into $\pi^+\pi^- J/\psi$ [40].

Together with the observed $Y(4008)$ and $Y(4660)$ states, one can see that there is a clear over-population of 1^{--} states above the four GeV energy region. The latter could be the predicted 3^3D_1 charmonium state. No additional 1^{--} states up to seven GeV were found in a Belle search [41].
Despite their partial overlap, there seems to be no mixing between the states since only $Y(4008)$ and $Y(4260)$ decay into $\pi^+\pi^- J/\psi$, whereas $Y(4360)$ and $Y(4660)$ decay into $\pi^+\pi^-\psi(2S)$. Neither of them has been observed in the other channel. Also no mixing between ψ and Y states has been observed so far [41].

These observations have stimulated a lot of research for the possible explanations of their nature. From possible non-resonant interpretations like interferences between continuum and well-known ψ resonances, conventional charmonium through distortions of the spectrum from $D^{(*)}\bar{D}^{(*)}$ hadron loops over tetraquarks to hybrids, all interpretations are being investigated. Other possible interpretations include hadro-charmonium, which is a charmonium surrounded by a light meson cloud and di-meson molecule interpretations like $D_1\bar{D}$. For a more detailed discussion please see [33] and references therein.

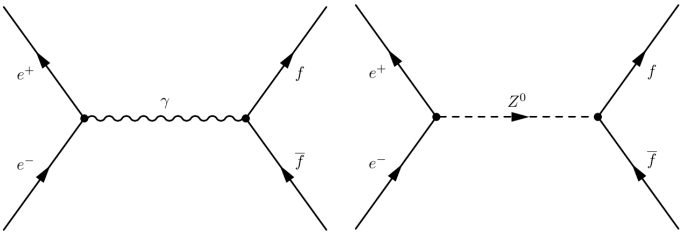

Figure 4: Feynman diagrams for hadron production in e^+e^- collisions

The hybrid interpretation is the most common interpretation since it is consistent with all measured values so far. The lowest lying 1^{--} hybrid was calculated from Lattice QCD to have a mass around 4.3 GeV. Because of the intrinsic gluon it should not couple to virtual photons, which would explain the dip of the R-scan and the small measured partial decay width into electrons, which is a factor 100 smaller than for conventional charmonium [41].

2.7 Hadron production in e^+e^- Collisions

Heavy quarkonia can be produced by collider or fixed target experiments such as proton-proton (LHC), proton-antiproton (Tevatron, future $\overline{\text{P}}$ANDA experiment) and e^+e^- colliders. The BESIII experiment, which will be further explained in chapter 3, uses the latter technique and has advantages as well as disadvantages compared to the other methods. Since electrons have no substructure and their interactions are well understood, they can be used for precision measurements. The initial state is known precisely as well as the energy of the collision, only small radiative tails can arise from initial state radiation and bremsstrahlung. Due to energy loss from synchrotron radiation ($\Delta E \sim 1/m^4 R$) the beam energy in a circular collider is limited. Light particles like electrons and positrons have much larger energy loss than protons and is smaller the bigger the radius R of the accelerator is.

In an electron-positron annihilation a virtual intermediate state which is a virtual photon or a virtual Z boson is formed as shown in the Feynman diagrams in Figure 4. The latter process can be neglected since for center of mass energies below the Z mass (∼90 GeV) the annihilation proceeds almost exclusively via the virtual photon. The photon has quantum numbers $J^{PC} = 1^{--}$ so all initially produced particles must have the same quantum numbers due to the conservation laws discussed in section (2.2). Therefore all vector charmonium states like J/ψ and ψ can be produced directly. All of them are summarized in the second column of the charmonium spectrum in Figure 1.

States with different quantum numbers can be populated by transition between the different states. Two different electromagnetic transitions must be distinguished : An emitted particle carries away angular momentum and due to angular momentum conservation the initial state has to change itself to another state to conserve angular

momentum. In the change of angular momentum from the initial to the final state, the lowest order multipole radiation are usually more likely to occur and dominate the transition, since the transition rates decrease by a factor of about 1000 from one multipole to the next higher order one [5]. In general, electric (charge) radiation or magnetic (moment) radiation can be classified into multipoles Eλ (electric) or Mλ (magnetic) of order 2^λ, e.g., E1 for electric dipole, E2 for quadrupole, or E3 for octupole radiation. The difference between electric and magnetic dipole coupling can be classified in terms of different parity. In E1 transitions the internal parity from the initial to the final state changes, whereas for M1 transitions it stays the same. An example for an E1 transition would be the decay of the $\psi(2S)$ via photon emission to the 1^{++} χ_{c1} state. A transition to the h_c 1^{+-} via a neutral pion π^0 would be called an M1 transition.

In $p-p$ or $p-\bar{p}$ machines the particles also interact via the strong interaction This means that partons inside the proton which carry only a fraction of the colliding energy interact so that the initial state has many more degrees of freedom, since many more particle take part in the collision. Therefore the initial state is not precisely known. This feature makes the analysis of final states much more complicated, but also allows to study glue-rich environments and all non-exotic quantum numbers can be produced directly.

2.8 Luminosity

The center of mass energy of an experiment only determines whether a physical process is possible. To get information about how often a certain process occur ones uses the value luminosity. The cross section σ determines the probability of a physical process at each energy point, whereas the production rate for a process of interest is given by $dN/dt = \mathcal{L} \cdot \sigma$ with $\mathcal{L}$ is the luminosity of the accelerator which depends on properties of the beam. It is given by

$$\mathcal{L} = \frac{N_1 N_2 f}{4\pi\sigma_x\sigma_y} \tag{4}$$

here N_1, N_2 are the number of particles per bunch, σ_x, σ_y is the spatial dimension of a bunch which is basically the cross section area of the overlap of both bunches and f the frequency of bunch collisions of the accelerator. The integrated luminosity is given by $\mathcal{L}_{int} = \int \mathcal{L} dt$ and classifies the amount of data taken during a specific time in experiments.

3 The BESIII Experiment

The Beijing Spectrometer III (BESIII) is the only detector at the Beijing Electron Postitron Collider (BEPCII) located at Beijing, China at the Institute of High Energy Physics (IHEP) of the Chinese Academy of Sciences. Electrons and positrons are accelerated in the BEPCII with a circumference of 237.5 m, covering the τ-charm energy region with energy ranges of $\sqrt{s}$=2-4.6 GeV, and collide at the interaction point (IP), see Figure 5, where the BESIII Experiment is located. It is an double ring multi-bunch collider operating since 2009 as an upgrade of the BEPC machine with a design luminosity of $10^{33}cm^{-2}s^{-1}$ [42]. This allows for collection of large data samples and therefore for precision measurements like rare decays in the non-perturbative QCD region. The BESIII experiment has collected the world largest data samples of J/ψ events with more than 1 billion events as well as the largest data sample of $\psi(2S)$ ($\sim 0.6 \cdot 10^9$), $\psi(3S)$, Y(4260) and Y(4360) events collected so far.

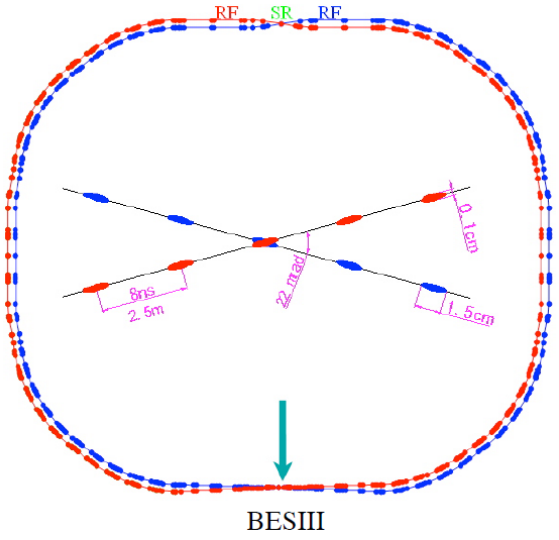

Figure 5: The BEPCII accelerator with the two colliding rings consisting of multiple Dipol- and Quadrupol magnets is shown here. There is a small crossing angle between the beams to get the highest possible luminosity.

3.1 The BESIII Detector

The technical design of the detector is optimized for expected data rates from BEPCII with an expected average momentum of about 0.3 GeV for charged particles, photon energies of about 100 MeV and the average multiplicity of 4 particles per Event [42].

As usual for symmetric high energy particle detectors, BESIII has an onion-shell like structure, with the innermost detector being a drift chamber for tracking , Time of Flight Detector and electro-magnetic calorimeters for particle identification surrounded by a magnet for the charge identification of the tracks and the outermost detector for muon identification as can be seen in Figure 6. More details of the detector elements are given in the following subsection.

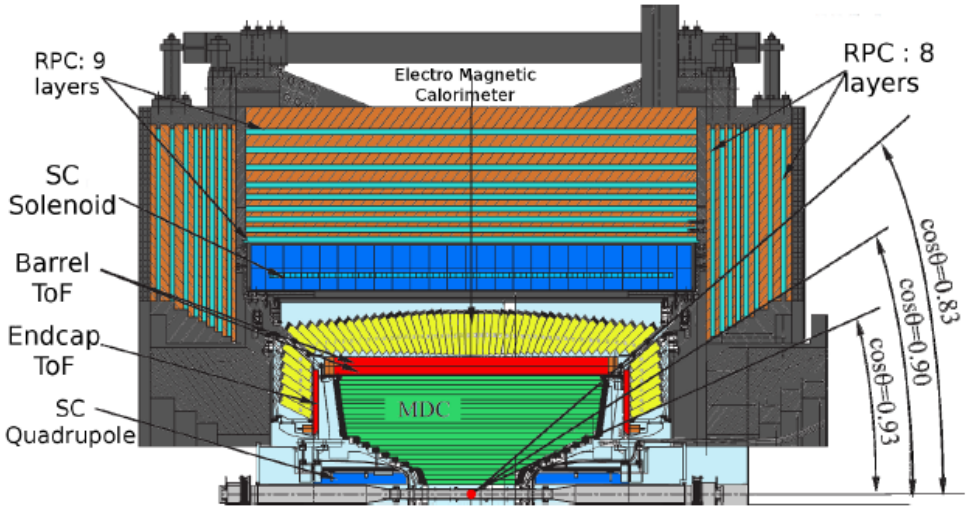

Figure 6: A schematic view of the upper half of the BESIII detector from [8].

3.1.1 Mini Drift Chamber (MDC)

The MDC as the innermost detector has to reconstruct tracks of charged particles with a good reconstruction efficiency, from measuring the bending of the tracks in the magnetic field it determines the charge and the momentum as well as the energy loss (dE/dx) of the particle traversing the chamber. Signals of the drift chamber are used as a level 1 trigger to select events.
To minimize multiple Coulomb scattering and secondary interactions the material around the IP has to be reduced as much as possible and it should have a maximum solid angle coverage of almost a 4π to measure charged tracks. The drift chamber has small-cells and low material density to reduce multiple scattering using a helium-based gas mixture (60% He / 40 % C_3H_8) with a spatial resolution of 135 μm averaged over the cell, a transverse momentum resolution of about 0.5 % at 1 GeV for charged particles and a dE/dx resolution of better than 6% for π/K separation up to 600 MeV at the 3 σ-level [43].
It is build from drift cells with almost square shape arranged in 43 circular layers, where the eight inner layers have higher granularity and less ageing effect gained by smaller cell sizes than the outer layers. Each layer contains of alternating field and sense wire layers, if a charged particle reaches the chamber gas atoms and molecules are getting ionized, the secondary electrons get accelerated to the sense wire. This additional energy leads to further ionization, a shower is produced and a current pulse can be measured. The additional field wires hold the electrical field in the drift volume constant, from the linear relation between the location of the first ionisation and the drift time, the track can be reconstructed.
All together the inner diameter of the drift chamber is 118 mm and the outer one is 1620 mm with a total length of about 2.6 m which covers a polar angle of $|cos\theta|<0.93$ and has a total acceptance of 93 % of 4 π [42].

3.1.2 Time of Flight Detector (ToF)

The Tof detector is made of a barrel with a polar angle coverage of $|cos\theta|<0.82$ with a radius of 81 to 92.5 cm and an endcap from $0.85<|cos\theta|<0.95$, the total length is 2.3 m for the barrel part [42].
The system is based on plastic scintillators, which are read out by photomultipliers. ToF measures the flight time t_m of a charged particle for particle identification which is related to the mass of the particle m, where L is the flight path and v the velocity of light:

$$\beta = \frac{L}{vt_m} \qquad m^2 = p^2\frac{1-\beta^2}{\beta^2} \quad . \tag{5}$$

The time of flight of charged particles is used for particle identification by comparing the measured time against the predicted time, which one can get from the tracking and momentum information from the drift chamber.
For the flight time measurement the scintillation principle is used: the ionizing particles excite molecules in the scintillator, when they de-excite light is emitted which can then be measured by the photomultiplier.
From the flight path the flight time difference of particles of different types can be obtained for particle discrimination, but this is limited due to the time resolution. The single layer time resolution for 1 GeV muons is 100-110 ps, this increases by 20% for kaons and pions, because of their strong interactions, whereas the double layer design was expected to have a total time resolution of 80-90 ps. The total time resolution for pions and kaons is in the order of 135 ps and therefore allows π/K separation at a 2σ level up to momenta of 1 GeV as determined in [44].

3.1.3 Electromagnetic Caloriemeter (EMC)

Its purpose is the detection of photons from 20 MeV up to about 2 GeV and electron/pion discrimination. For that purpose a high energy resolution, a good position resolution and high efficiency is needed.
Electrons, positrons and photons produce an electromagnetic shower in the EMC and deposit their whole energy in the detector volume while getting stopped in the material. Their ratio of deposited energy and total momentum is nearly 1 as their masses are so low [2]. Electrons and positrons can be separated from photons with the help of the MDC tracks, because neutral particles do not produce signals within the MDC. Muons pass the EMC, they are not stopped in the material and deposit only a small fraction of their energy in the crystals.
The BESIII EMC consists of a barrel and two endcap parts ($0.85< |\cos(\theta))|<0.93$) covering 93% of 4 π. Both are built of thallium doped caesium iodide (CsI(Tl)) scintillating crystals. The crystal length is 28.5 cm (corresponding to 15.1 radiation lengths X_0) and is read out by two photo diodes mounted on the top of a crystal. The entire calorimeter has 6272 CsI(Tl) crystals with a total weight of about 24 tons.
For Bhabha events at $\sqrt{s}$ =3.686 GeV the energy resolution was measured to be 2.3% in the barrel and 4.1% in the endcap system. For photons the resolution is 2.7% for the barrel and 4.2% for the endcap systems, respectively [45]. The position resolution for photons with an energy of 1 GeV is 6 mm in the barrel region and 9

mm in the endcap region.

3.1.4 Superconducting Solenoid Magnet (SSM)

The SSM provides a uniform axial magnetic field with a strength of 1.0 Tesla to measure the accurate momentum of a particle. It encloses the 3 innermost sub-detectors; the inner radius is limited by the EMC 1.38 m, the outer one is 1.7 m. The SSM is cooled with liquid He with a temperature of 4.5 K and has a nominal current of 3369 A [42].

3.1.5 Muon Chamber

Most of the hadrons passing through the EMC will get stuck somewhere in the absorber material of the magnetic field's return joke and will produce a hadronic shower near the layers where the interaction did occur [43]. Muons with a high momentum are minimal ionizing particles. They mostly cross all the layers of the muon chamber and produce one signal in each of the layers. The main goal of the muon identification system is to separate muons from charged pions and other hadrons based on their hit patterns in the detector. It has an detection efficiency of 98%.
The Muon Identification System is a gaseous detector based on Resistive Plate Chambers (RPCs) and consists of eight detecting layers in the endcap ($0.75< |\cos(\theta)| <0.89$) and nine in the barrel ($|\cos(\theta)|<0.75$). The whole system is embedded in the magnetic flux return and each layer is made of two RPC layers and one pickup strip layer which are compacted as a sandwich. The thickness of the steel plates in between the chambers is varying from 3 cm up to 15 cm, where the first layer of steel plates are the thinner ones. This ensures that the cut-off momentum for muon detection, which is around 400 MeV/c [42], is as small as possible.

3.2 The BESIII Offline Software System (BOSS)

BOSS [46] is developed using object-oriented C++ language. The software uses some external HEP libraries such as CERNLIB, CLHEP, ROOT etc and also reuses parts of code from Belle, BaBar, ATLAS and GLAST experiments [47].
The whole data processing and physics analysis software is divided into five sub-projects: framework, simulation, calibration, reconstruction and analysis tools.

Framework The BOSS framework is a specific implementation of the GAUDI architecture, which was originally developed by the LHCb experiment. It provides the control of data processing, event data modelling, detector description, data management and other common services and utilities.

Simulation The BESIII Monte Carlo simulation generates events at the interaction point, propagates the resulting particles through the sub-detectors and records the response of all detector components to these particles. The simulation software

inherits about 30 different event generators allowing for accurate simulation of charmonium production and the subsequent decays. Its detector simulation is based on Geant4 (GEometry ANd Tracking) [48] that allows for the complete simulation of the BESIII sub-detectors.

Calibration The BESIII calibration software is implemented to produce calibration constants for each sub-detector by the calibration algorithm. It also provides a common way to obtain the constants stored in the persistent storage needed for the reconstruction algorithm.

Reconstruction Data reconstruction is the central task of offline data processing. The reconstruction software consists of a complete set of algorithms for event time determination, track finding from the individual hits in the MDC and fitting those, dE/dx and time of flight calculation for PID information, clustering and shower formation in the Calorimeter, tracking in the Muon Chamber. Here reconstructed tracks are matched with the information of the outer lying detectors to get the whole picture.

Analysis Tools The BESIII analysis software is the central algorithm for data analysis. From the reconstruction results it builds event data objects, which are more suitable for physics analysis. Moreover it provides various software tools that are needed for physics studies like the PID tools, kinematic fitting tools and the service for secondary vertex finding to improve momentum and mass resolution.

4 Analysis and Results

4.1 Motivation

In this analysis a search for the final state $X(3872) \to J/\psi\gamma$ is investigated with data sets from the BESIII experiment.

Since the $X(3872)$ is a 1^{++} state, the idea is to search for radiative transition of excited vector charmonium or charmonium-like states such as $Y(4260)$ and $Y(4360)$ to $X(3872)$[1], which then decays to $J/\psi\gamma$. These exotic states need to be investigated in other than the known decay processes from the PDG to better understand their nature. Especially the search for radiative decays is of great interest for theorists and was already proposed in [49]. The process $Y(4260)/Y(4360) \to X(3872)\gamma$ is unique to understand the exotic features of both the $X(3872)$ as well as the $Y(4260)$ and $Y(4360)$ states. Moreover it is of great importance to obtain connections between those exotic XYZ states to further understand their nature.

Recently BESIII published a search for this radiative decay in the final state $X(3872) \to J/\psi\pi^+\pi^-$ [1]. For the first time we observed the $X(3872)$ in the process of $e^+e^- \to \gamma X(3872)$ with a significance of 6.3 σ, which is the first production in the charm sector. Before that the $X(3872)$ was only observed in B-meson decays and hadron collisions. The most important results are summarized in the next paragraph, for further information see [1].

The fit result of BESIII is shown in Figure 7 (left) which gives a mass of $M(X(3872)) =$

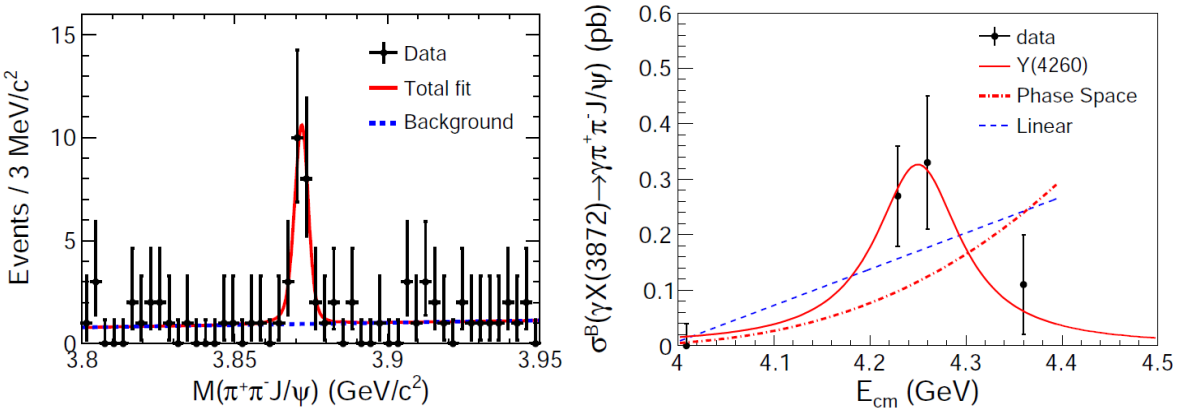

Figure 7: left: Fit of the $M(J/\psi\pi^+\pi^-)$ distribution, right: Fit to cross section with $Y(4260)$ resonance [1].

$3871.9 \pm 0.7\ MeV/c^2$ and 20.1 ± 4.5 signal events for the whole data set. The product of the Born-cross section times the branching fraction for various data sample are summarized in Table 2. For measurements where the $X(3872)$ signal is not statistically significant, upper limits at 90 % C.L. are given.

To test if the $X(3872)$ really originates from a radiative decay of $Y(4260)$ or $Y(4360)$, the measured cross sections at different energy points are shown on the right side of Figure 7. Three different functions are fitted to the data: a linear con-

$\sqrt{s}$(GeV)	N^{obs}	N^{up}	$\sigma^B \cdot \mathcal{B}$(pb)	$\sigma^{up} \cdot \mathcal{B}$(pb)
4.009	0.0 ± 0.5	< 1.4	$0.0 \pm 0.4 \pm 0.01$	< 0.11
4.229	9.6 ± 3.1	-	$0.27 \pm 0.09 \pm 0.02$	-
4.260	8.7 ± 3.0	-	$0.33 \pm 0.12 \pm 0.02$	-
4.360	1.7 ± 1.4	< 5.1	$0.11 \pm 0.09 \pm 0.01$	< 0.36

Table 2: Summarized Results of cross section measurements of $\sigma^B[e^+e^- \to \gamma X(3872)] \cdot \mathcal{B}(X(3872) \to J/\psi\pi^+\pi^-)$ from [1].

tinuum, a phase-space function and the $Y(4260)$ resonance, latter describes the data better than the other options. However the current statistic is not enough to rule out continuum production of the $X(3872)$ and the existence of the radiative decay is still unclear. If this decay can be confirmed, this would have important implications for the common features in the nature of both states. Therefore different final state searches for the $X(3872)$ have to be done, one of them is presented in this thesis.

According to previous measurements done by Belle and *BABAR* , the branching fraction was obtained to be

$$\mathcal{B}(X(3872) \to \gamma J/\psi) \times \mathcal{B}(B^+ \to K^+ X(3872)) = (1.78^{+0.48}_{-0.44} \pm 0.12) \times 10^{-6} \quad [25]$$
$$\mathcal{B}(X(3872) \to \gamma J/\psi) \times \mathcal{B}(B^+ \to K^+ X(3872)) = (2.8 \pm 0.8 \pm 0.1) \times 10^{-6} \quad [31]$$

while *BABAR* also measured

$$\mathcal{B}(X(3872) \to J/\psi\pi^+\pi^-) \times \mathcal{B}(B^+ \to K^+ X(3872)) = (8.4 \pm 1.5 \pm 0.7) \times 10^{-6}$$

[50]. This leads to a branching ratio of

$$\frac{\mathcal{B}(X(3872) \to J/\psi\pi^+\pi^-)}{\mathcal{B}(X(3872) \to \gamma J/\psi)} \approx \frac{1}{3}.$$

Due to the observation of 20.1 ± 4.5 signal events by BESIII in $X(3872) \to J/\psi\pi^+\pi^-$ [1] about seven events are expected for the $X(3872) \to \gamma J/\psi$ channel, since the MC simulation efficiencies are comparable.

4.2 Data Sets and Monte-Carlo Simulation

The center-of-mass (CM) energies and corresponding integrated luminosities used in this analysis are given in Table 3. The Monte Carlo (MC) simulation and data analysis was done with BOSS software version 663p01 and the data has been collected in the run period from 2011 until summer 2012.

The optimization of event selection criteria and the estimation of background are performed with MC simulations. The MC production is based on the KKMC generator [51] which uses calculations of electroweak processes from the SM, for example the process $e^+e^- \to f\bar{f} + n\gamma$ with f being fermions (leptons, quarks). KKMC includes ISR effects and radiative corrections and is used to generate charmonium

$\sqrt{s}$(GeV)	Luminosity (pb^{-1})
4.229	1094
4.260	827
4.360	545

Table 3: The CM energies and luminosities from the data used for this analysis

QED:	$e^+e^- \to e^+e^-$
	$e^+e^- \to \mu^+\mu^-$
	$e^+e^- \to \tau^+\tau^-$
	$e^+e^- \to \gamma\gamma$
continuum:	$e^+e^- \to q\bar{q}(u,d,s)$
ISR:	$e^+e^- \to \gamma_{ISR}J/\psi$
	$e^+e^- \to \gamma_{ISR}\psi(2S)$
	$e^+e^- \to \gamma_{ISR}\psi(3770)$
	$e^+e^- \to \gamma_{ISR}\psi(4040)$

Table 4: Summary of non-resonant inclusive $Y(4260)$ MC background samples used in the analysis.

resonances. The decay of charmonium is modelled using the EvtGen package [52]. The GEANT4-based simulation software [53] covers the geometric description of all BESIII sub-detectors and the detectors behaviour to traversing particles.

In order to determine the detection efficiency and to optimize selection criteria, the exclusive decay $e^+e^- \to \gamma X(3872)$ with $X(3872) \to J/\psi\gamma$ is simulated at each CM energy point mentioned in Table 3. Here the phase space model is used to simulate the decay $e^+e^- \to \gamma X(3872)$ as well as $X(3872) \to J/\psi\gamma$, where the J/ψ decays into e^+e^- and $\mu^+\mu^-$ with identical branching ratio modelled with the VLL model (vector decaying into two leptons). Final State Radiation(FSR) effects associated with leptons is handled by PHOTOS and also included in the MC simulation. Each MC sample contains 20000 events.

For background studies an inclusive Y(4260) MC sample corresponding to 500 pb^{-1} integrated luminosity is used. It includes physical processes like QED, ISR of vector charmonium states given in Table 4 and resonant contributions given in Table 5. Those events are generated with KKMC, the main known decay modes are generated with EvtGen, while the branching fractions are set to the world average values according to [2]. The background at the other energy points is expected to be similar, therefore only inclusive background samples at 4260 MeV CM energy are used.

$D\bar{D}$	$Y(4260) \to D\bar{D}, D^*D, D^*D^*, D_s\bar{D}_s, D_s^*D_s, D_s^*D_s^*$
XYZ	$Y(4260) \to \gamma\chi_{c0}, \gamma\chi_{c1}, \gamma\chi_{c2}, \gamma\eta_{c2}, \gamma Y(3940), \gamma X(3940),$ $\gamma\chi_{c0}(2P), \gamma\chi_{c1}(2P), \gamma\chi_{c2}(2P)$
Hadrons	$Y(4260) \to \pi^+\pi^- J/\psi, \pi^0\pi^0 J/\psi, \pi^+\pi^-\psi(2S), \pi^0\pi^0 J/\psi,$ $\pi^0\pi^0\eta J/\psi, \pi^+\pi^-\pi^0 J/\psi, \pi^+\pi^-\pi^0\eta\eta J/\psi, \eta J/\psi, \eta' J/\psi,$ $\pi^0 J/\psi, K^+K^- J/\psi, \omega\chi_{c0}, \pi^+\pi^-\pi^0\chi_{c1}, \pi^+\pi^-\pi^0\chi_{c2}, \phi\pi^+\pi^-$
$D\bar{D}\pi$	$Y(4260) \to D^*D\pi, D^*D^*\pi$

Table 5: Summary of resonant inclusive $Y(4260)$ MC background samples used in the analysis.

4.3 General Event Selection Criteria

For this study the events of interest are $X(3872) \to J/\psi\gamma$ while J/ψ is reconstructed with lepton pairs $(e^+e^-, \mu^+\mu^-)$. Therefore all signal events should have two oppositely charged tracks and at least two neutral tracks corresponding to the two photons. The radiative E1 photon has about 400 MeV which is far above the lower threshold of the detector. The following event selection criteria are applied to both MC and data samples.

Charged Tracks are reconstructed from their MDC information and the following cuts are applied:

- Each charged track is required to originate from the interaction point therefore it has to satisfy $V_{xy} = \sqrt{{V^2}_x + {V^2}_y} < 1$cm perpendicular to the beam axis and $|V_z| < 10$ cm in direction to the beam axis. Here V_i are the coordinates of the point of the closest approach to the run dependent interaction point of each track.

- All charged tracks are required to lie within the polar angle region of $|\cos\theta| < 0.93$ due to the geometry of the BESIII detector.

- Events with only two oppositely charged tracks with a total charge of zero are kept fur further analysis.

Neutral Particles are reconstructed from their EMC information if the photon candidates full fill the following selection:

- The deposited energy in the barrel EMC ($|\cos\theta| < 0.8$) is larger then 25 MeV.

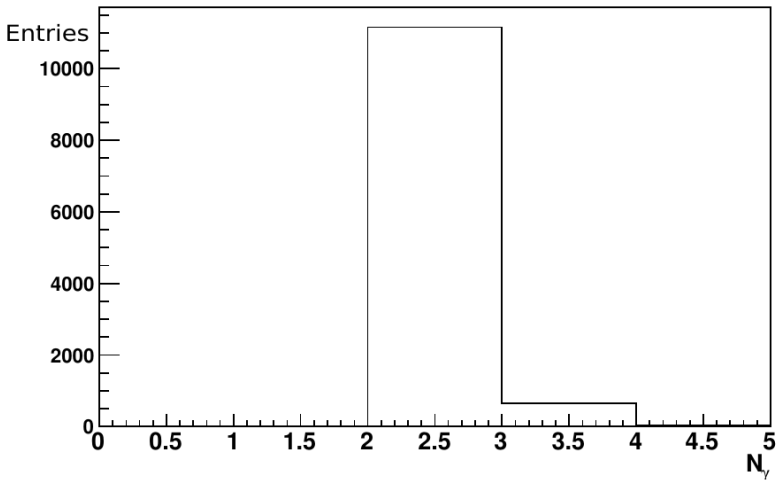

Figure 8: Number of photons per event from Signal MC at $\sqrt{s} = 4260$ MeV.

- Showers in the endcap EMC ($0.86 < |\cos\theta| < 0.92$) must have at least 50 MeV. This is done to suppress background and noise not coming from the photons.
- Photons produced by bremsstrahlung are rejected by the requirement that the angle between charged particles and a photon should be larger than 20°.
- To suppress electronic noise and energy deposits which are unrelated to the event, the EMC signal has to be within zero to 700 ns after the collision.
- Events with at least two neutral tracks are kept for further analysis. In Figure 8 the number of photons in exclusive signal MC at $\sqrt{s} = 4260$ MeV is shown.

Particle Identification has to be done for charged tracks to distinguish electrons and muons. The separation is determined by comparing the energy deposited in the EMC from both particles as can be seen in Figure 9 for exclusive MC samples at $\sqrt{s} = 4260$ MeV. Muons deposit only a small fraction of their energy in the EMC since they are minimal ionizing particles and traverse also the outer muon chambers, their distribution has a maximum around 0.2 GeV compared to Figure 9. Electrons are getting stopped and deposit all their energy in the EMC which corresponds to the smooth distribution starting at one GeV in Figure 9. Therefore electrons are required to have $E_{EMC} > 1$ GeV and for muons a cut of $E_{EMC} < 0.35$ GeV is used. The momentum measured by the MDC should be bigger than one GeV for leptons. This cut helps to suppress background from possible pions in the data samples.

Kinematic fits are done to further reject the background and to take into account momentum and energy conservation. First of all vertex fitting is used to constrain the two charged particles in each final state to the same starting point. Furthermore a four-constraint (4C) kinematic fit is performed with momentum and energy conservation of $\gamma\gamma J/\psi$ to improve the resolution. The fit constraints are the initial 4-momenta of each neutral and charged track. The fit takes into account the

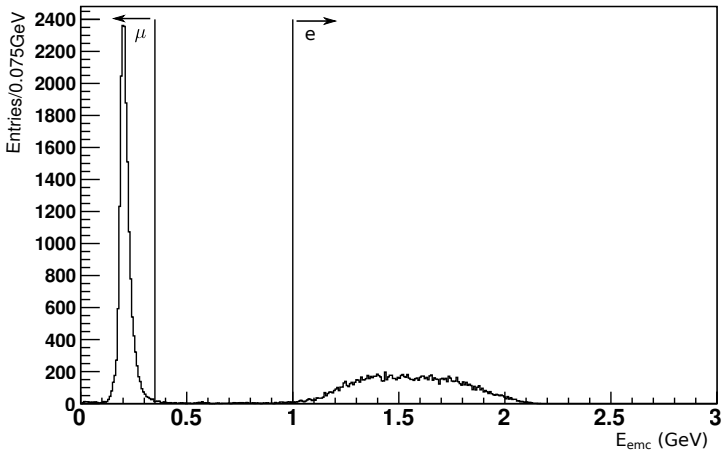

Figure 9: Lepton energy deposition in the EMC for signal MC at $\sqrt{s} = 4.260$ GeV. Cut lines are drawn to discriminate muons (left) and electrons (right).

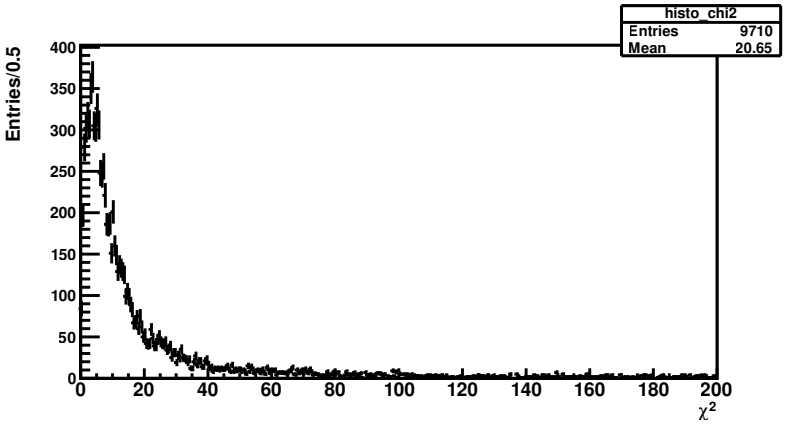

Figure 10: The 4C kinematic fit χ^2 distribution for exclusive signal MC at $\sqrt{s} = 4260$ MeV.

4-momentum vectors for both leptons, either being electron positron or muon anti-muon, and every combination of photons. For events with more than two photons in one event, the best combination corresponding to the smallest ${\chi^2}_{4C}$ is chosen by looping all $l^+l^-\gamma\gamma$ combinations. The χ^2 distribution of the 4C fit is shown in Figure 10. For the further event selection $\chi^2 < 60$ is required. The efficiency of the 4C fit is quite high with $85.7 \pm 0.2\%$ of simulated MC events pass this selection criteria (see Table 6), where the error is the binomial one calculated from $\Delta\epsilon = \sqrt{N\epsilon(1-\epsilon)}/N$, it takes into account the correlation of the selected and total events N [8].

4.4 Specific Event Selection Criteria

In Figure 11 the J/ψ from MC samples at $\sqrt{s} = 4260$ MeV is shown. In the MC simulation the J/ψ resonance is produced with mean and width set to the values of the PDG ($\mu = 3.0969$ GeV, $\Gamma = 93$ keV)[2]. The invariant mass spectrum is fitted with a double Gaussian function to extract the resonant J/ψ parameters, which are then fixed in the fit to the data and also to determine the detector resolution. The fit results give a central value of 3.0998 GeV and a width of σ ∼8.1 MeV, which gives a detector resolution of ∼8 MeV.
This Fit and all following fits are done with the RooFit package included in ROOT. It is capable to do unbinned maximum likelihood fitting, which is more stable compared to other fitting routines, where only binned fits can be performed. The minimizer Minos is used for finding the maximum likelihood and to obtain asymmetric error bars for the fitted quantities.

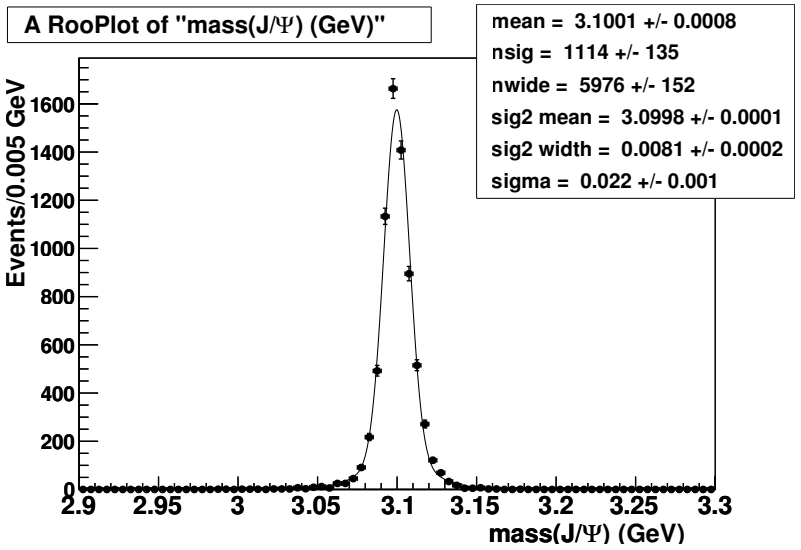

Figure 11: Invariant mass distribution of lepton pairs from MC simulation at $\sqrt{s} = 4260$ MeV with a double Gaussian fit.

Figure 12 shows an example of the invariant mass of lepton pairs at $\sqrt{s} = 4230$ MeV after the mentioned event selection criteria. A clear J/ψ can be seen on top of high background contributions, which is the same for the other data samples. The invariant mass spectrum is fitted with a double Gaussian function with the resonant parameters fixed to the values obtained from Figure 11 and a linear background function. The result is shown in Figure 12. In order to select further J/ψ events for the $X(3872)$ reconstruction, a mass window of $3.074 < m(l^+l^-) < 3.1024$ is used which corresponding to 3σ region of the J/ψ signal.

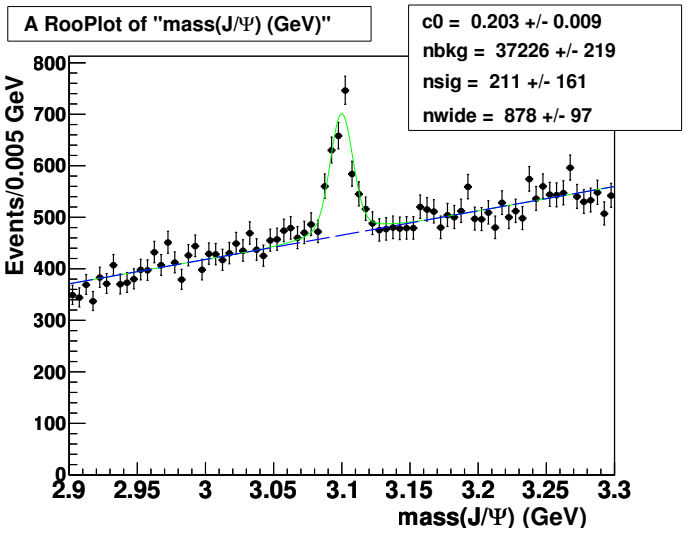

Figure 12: Double Gaussian and linear background function fit to the invariant mass distribution of lepton pairs from data taken at $\sqrt{s} = 4260$ MeV.

In Figure 13 the invariant mass spectrum of both photons is shown for data after applying all above requirements including the J/ψ mass window. A clear η peak in the data can be observed for each data sample. In order to reject $e^+e^- \to \eta J/\psi$ background events, a veto for η events is used to reject this background for the final selection. In Figure 14 the η signal is fitted with a Gaussian to get its mean value and

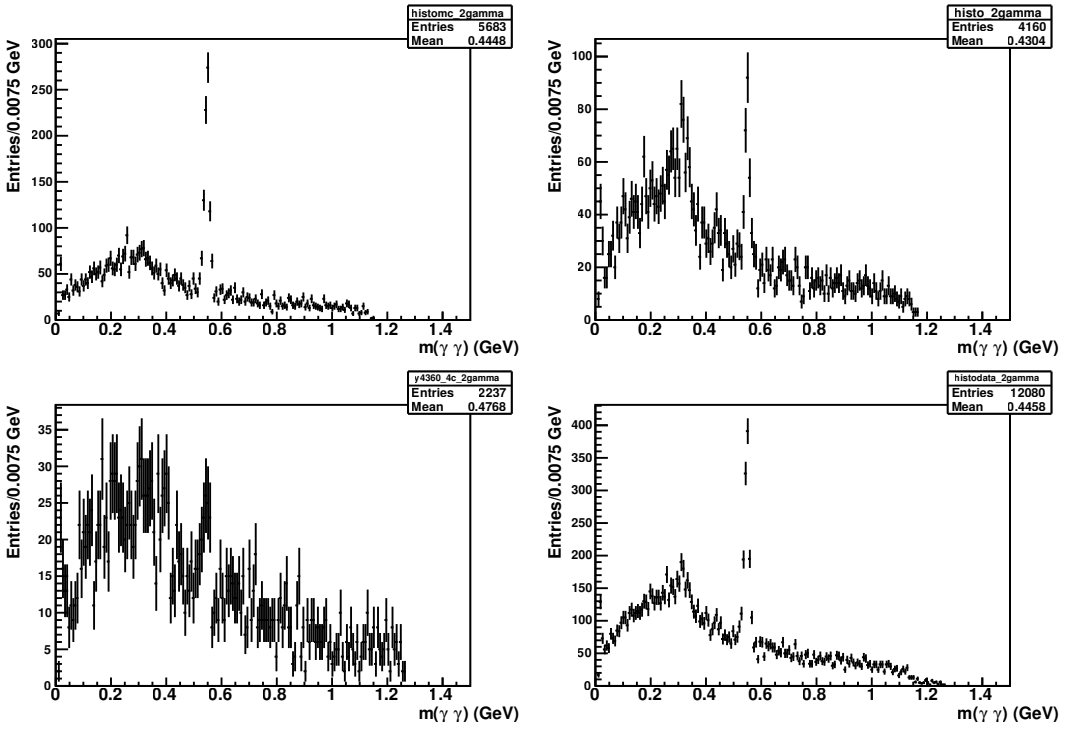

Figure 13: Invariant mass distribution of both photons for data samples taken at $\sqrt{s} = 4.230$ GeV (top left), at $\sqrt{s} = 4.260$ GeV (top right), at $\sqrt{s} = 4.360$ GeV (bottom left) and the sum off all data samples (bottom right).

standard deviation, a second order polynomial is used to describe the background. From the fit the center is determined to be 0.5475 GeV and the standard deviation to be 9 MeV. This values are used to determine the η-veto as a 3σ surrounding around the central mass given as $|M(\gamma\gamma) - M_\eta|$ <0.027 GeV.

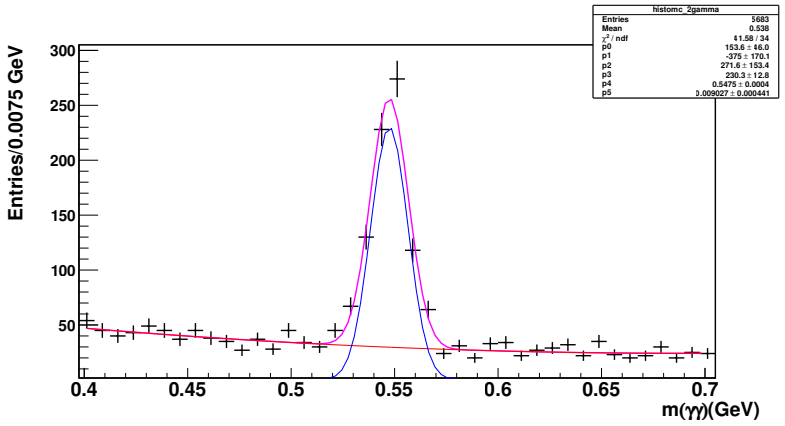

Figure 14: Fit of Gaussian to the invariant mass distribution of the two photons from data taken at $\sqrt{s} = 4.260$ GeV.

The electron mode in this analysis suffers from huge Bhabha background contributions. Exclusive Bhabha MC simulations were done at $\sqrt{s} = 4.260$ GeV and the distribution of the momentum of the leptons is shown in left of Figure 15. As expected the Bhabha background peaks at around 2 GeV due to the total electron/positron energy, whereas the exclusive MC has most events between 1.4 to 1.8 GeV as shown on the right side of Figure 15. To reject those events a total momentum cut of $1.2 < p_{lep} < 1.97$ GeV is used. In MC samples the amount of signal events removed by this cut is ∼8%, but almost all Bhabha background events are rejected.

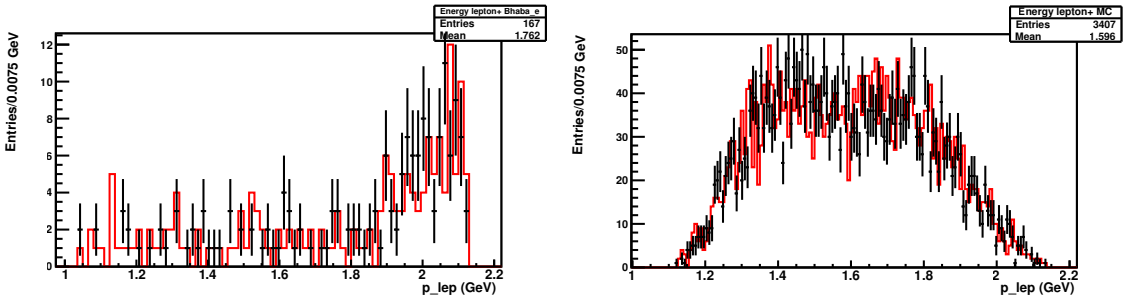

Figure 15: The momentum distribution of leptons from simulated Bhabha background compared to exclusive signal MC at $\sqrt{s} = 4.260$ GeV. Positively charged leptons are drawn in red, whereas the negatively charged ones are drawn in black.

Due to the kinematics of Bhabha events, they almost go back-to-back close to the beam pipe, as can be seen in left of Figure 16. In contrast, events from

signal MC simulation (right) are equally distributed over the whole polar angle range. To reject those events, the polar angle for electrons/positrons has to satisfy $\cos(\theta_{e^-}) \geq -0.6/\cos(\theta_{e^+}) \leq 0.6$ respectively. With this cut another 8% signal MC events are rejected.

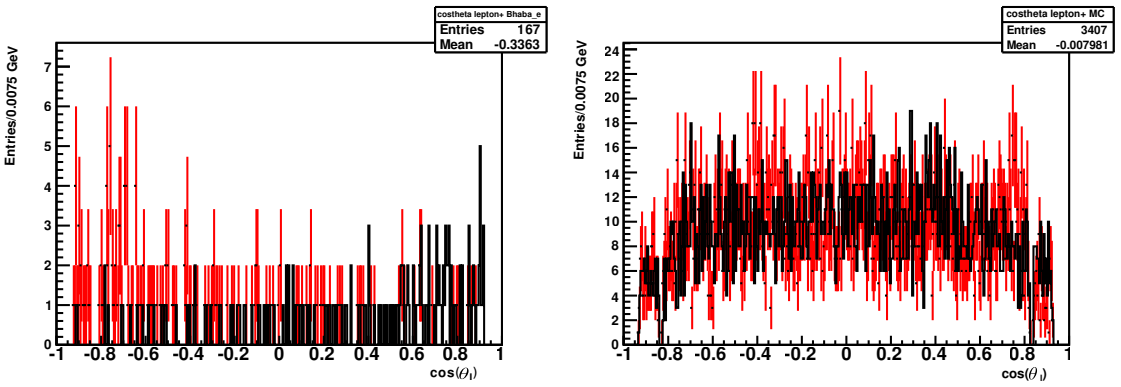

Figure 16: The polar angle of electrons from simulated Bhabha events (left) compared to exclusive signal MC (right) at $\sqrt{s} = 4260$ MeV. The distribution of positrons is drawn in red and the contribution of electrons is drawn in black.

In Figure 17 the spectrum of photon energy versus the polar angle for the higher energetic photon is shown from MC simulation at 4.26 GeV after the kinematic fit. Here one can see that the maximal energy of the higher energetic photon is 0.8 GeV, therefore a cut is set to this maximum energy to suppress further background. This cut removes almost no events ($< 1{\cdot}10^{-3}$) in MC with an efficiency of 99.9±0.7%.

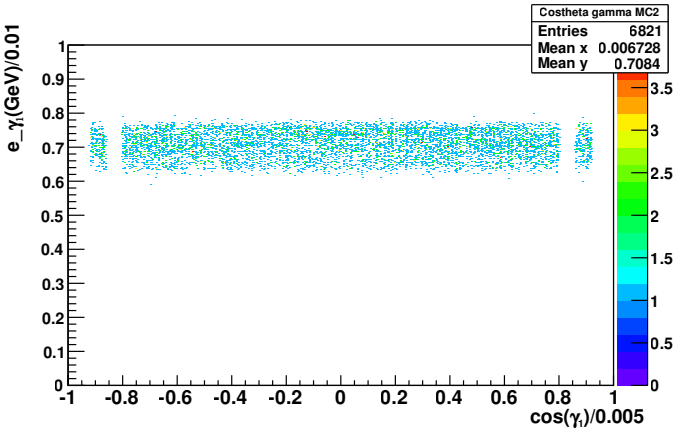

Figure 17: The polar angle of the higher energetic photon versus the energy of the photon is shown here from exclusive signal MC at $\sqrt{s} = 4260$ MeV.

After applying all final selection criteria explained above, the detection efficiencies from exclusive MC simulations are 34.4% at $\sqrt{s} = 4.229$ GeV, 34.0% at $\sqrt{s} = 4.260$ GeV and 33.1% at $\sqrt{s} = 4.360$ GeV. The cutflow of the final event selection is sum-

Cuts	$\sqrt{s} = 4.229$ GeV	$\sqrt{s} = 4.260$ GeV	$\sqrt{s} = 4.360$ GeV
total number	20000	20000	20000
Charged tracks	16674	16648	16597
Photon selection	11839	11839	11946
PID	11378	11403	11504
Vertex Fit	11297	11328	11427
4C-Kinematic fit	8903	8878	9051
η veto	8431	8430	8686
p_{lep} cut	7730	7736	7620
$\cos_e$ cut	7097	7098	6990
$e_{\gamma 1} \leq 0.8$ cut	7093	7091	6950
J/ψ cut	6810	6799	6625
Efficiency	34.4%	34.0%	33.1%

Table 6: The Cutflow from MC simulations

marized in Table 6.

After the final selection criteria, the $X(3872)$ signal simulated from exclusive MC is shown in Figure 18. Here the relation $m(J/\psi\gamma) - m(l^+l^-) + m(J/\psi)$ is used to cancel resolution effects of the leptons which is also used later for data. The invariant mass $m(J/\psi\gamma)$ is here obtained from the invariant mass of both leptons with the J/ψ mass cut combined with the higher energetic photon from the kinematic fit. This relation is always used in the following plots where the short form $m(J/\psi\gamma_{\mathrm{h}})$ is used as a caption.

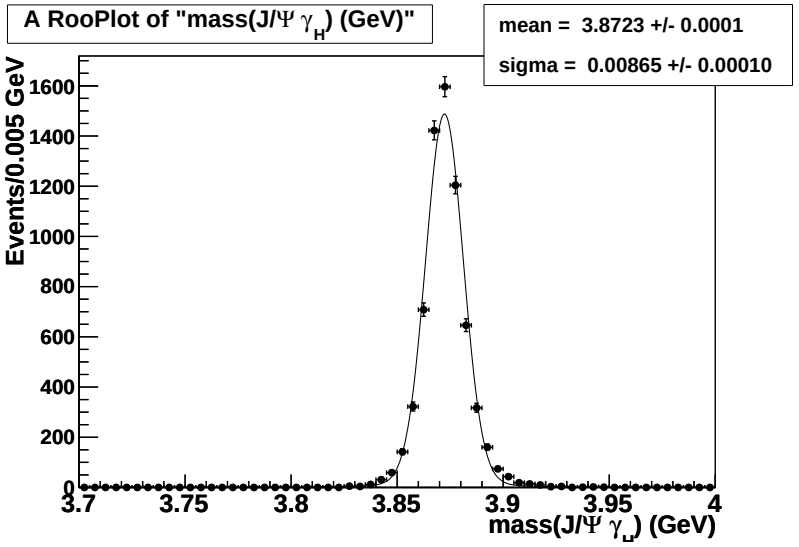

Figure 18: The $X(3872)$ signal from MC simulation at $\sqrt{s} = 4260$ MeV after all cuts. A fit is performed with a Breit-Wigner convolved with a Gaussian function to extract the resonance parameters.

The $X(3872)$ signal is fitted with a Breit-Wigner convolved with a Gaussian to get the resonant parameters which are then used to fit the data in the next section. The central value from the fit is $m(X(3872)) = 3.8723 \pm 0.0001$ GeV and the width is taken from the Gaussian to be $\sigma = 0.00865 \pm 0.00010$ GeV.

4.5 Results of Data Analysis

For the different data samples all discussed requirements are used to reject possible background contributions. Figure 19 shows the invariant mass distribution of the higher energetic photon and the two leptons after the J/ψ mass window requirement with the relation $m(J/\psi\gamma) - m(l^+l^-) + m(J/\psi)$ at different energy points. In the bottom right plot all data samples are added together.

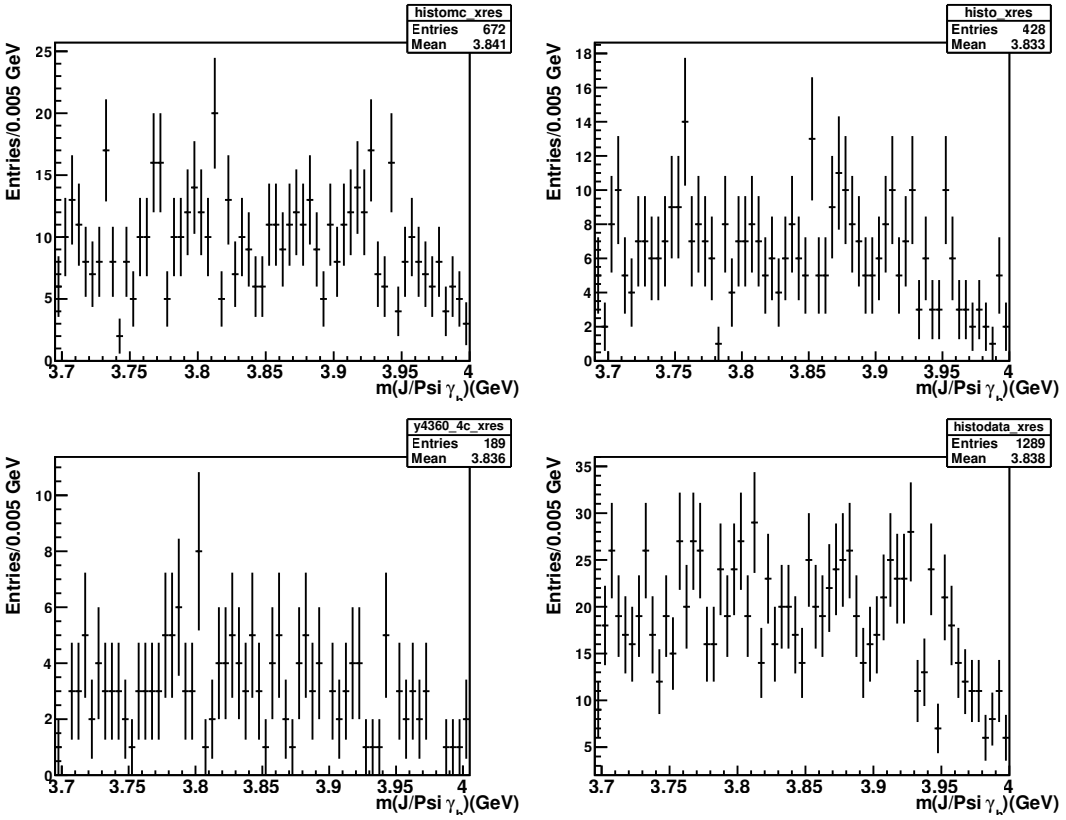

Figure 19: The invariant mass distribution of $m(J/\psi\gamma) - m(l^+l^-) + m(J/\psi)$ for all data samples with the final selection criteria is shown here. The top left plots shows data at $\sqrt{s} = 4.230$ GeV, the top right for $\sqrt{s} = 4.260$ GeV and bottom left shows it for $\sqrt{s} = 4.360$ GeV. The sum off all data is shown in bottom right.

I fitted the $m(J/\psi\gamma)$ signal with the same function which was used to fit the MC signal, a Breit-Wigner convolved with a Gaussian function, where the signal shape parameters are fixed to the one from MC but the mean is floating. These resonant parameters from signal MC at $\sqrt{s} = 4.260$ GeV are used for all data sets due to the similarity with the other energy points. For the background fit, a first order Chebyshev polynomial function is used. This can be done because of the non peaking background contributions, which are further discussed in the next section. The fit for the different data sets is shown in Figure 20 and the fit results are given in Table 7.

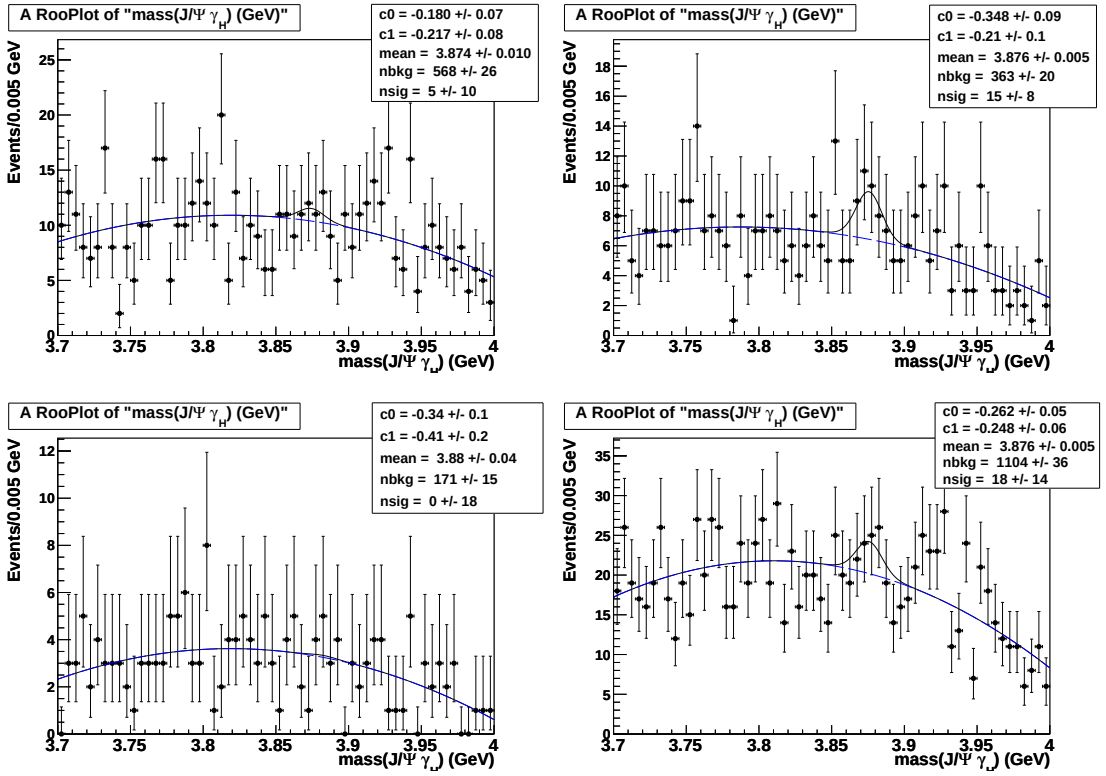

Figure 20: Fit to the invariant mass distribution of $m(J/\psi\gamma) - m(l^+l^-) + m(J/\psi)$ for all data samples with the final selection criteria are shown here. The top left plots shows data at $\sqrt{s} = 4.230$ GeV, the top right for $\sqrt{s} = 4.260$ GeV and bottom left shows it for $\sqrt{s} = 4.360$ GeV. The sum off all data is shown in bottom right.

$\sqrt{s}$(MeV)	mean value	number of signal events	significance
4229	$3874.34^{+9.78}_{-9.89}$	5.3 ± 9.8	0.57
4260	$3875.56^{+5.45}_{-5.54}$	14.5 ± 8.3	2.12
4360	$3882.92^{+31.03}_{-31.23}$	0.4 ± 5.3	0.09
sum of all data	$3875.72^{+5.81}_{-5.89}$	18.4 ± 13.5	1.59

Table 7: Fit results from the invariant mass spectrum of $m(J/\psi\gamma) - m(l^+l^-) + m(J/\psi)$ of Figure 20 for the different data samples

In the distributions of Figure 20 no clear $X(3872)$ signal is observed in each data set due to the still high background contamination in this channel, maybe there is a hint of a signal. The mean value for the $X(3872)$ signal is in agreement with the PDG [2] average of 3871.68 ± 0.17 MeV.
The statistical significance of the signal is estimated by comparing the difference of the log-likelihood value with signal and background and with only the background function in the fit ($\Delta(-2\ln\mathcal{L})$). This can be related to the significance by the use of Wilks theorem, which states that for a large sample size the probabiliy distribution of the test statistic : $\Delta(-2\ln\mathcal{L}) = -2\ln\frac{\mathcal{L}_\mathcal{B}}{\mathcal{L}_{\mathcal{S}+\mathcal{B}}}$ for a model will be asymptotically χ^2 distributed, with degrees of freedom equal to the difference in dimensionality of the

two models [54]. From this, one gets a significance of $S = \sqrt{\Delta(-2\ln\mathcal{L})}\sigma$ =1.59σ for the sum of all data sets, the other calculated ones are given in Table 7.

As a check for the $X(3872)$ signal, Figure 21 shows the $m(J/\psi\gamma)-m(l^+l^-)+m(J/\psi)$ mass distribution from $J/\psi \to \mu^+\mu^-$ mode and $J/\psi \to e^+e^-$ mode separately for the sum of all data events. The fit on the left for the muon mode gives a mean of 3.879 ± 0.005 and 11 ± 7 number of signal events, the statistical significance is calculated to be 2.1σ. For the electron mode (right) the fit gives 3.87 ± 0.01 and 8 ± 17 number of signal events with a significance of 0.67σ. The background contributions in the different modes are very different, the electron mode still suffers from much more background which could not be excluded through the cuts in the final selection criteria.

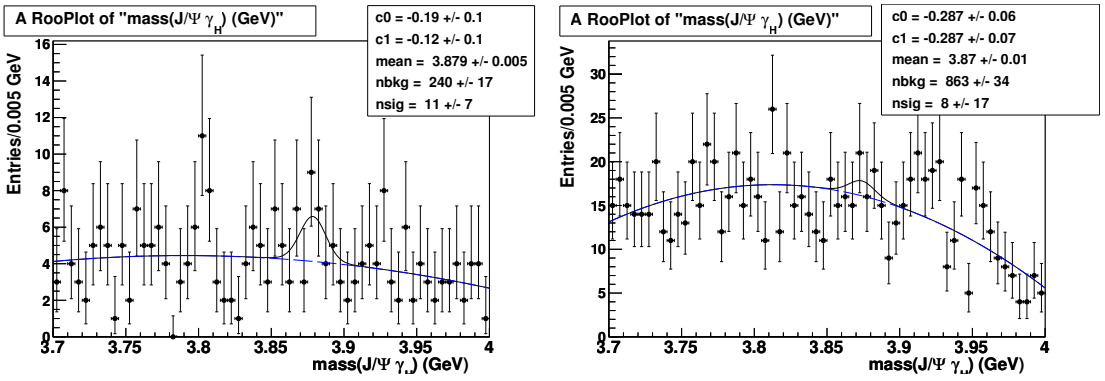

Figure 21: A Fit to the $m(J/\psi\gamma)-m(l^+l^-)+m(J/\psi)$ mass distribution in all data samples for $J/\psi \to \mu^+\mu^-$ (left) mode and $J/\psi \to e^+e^-$ (right) mode with all cuts.

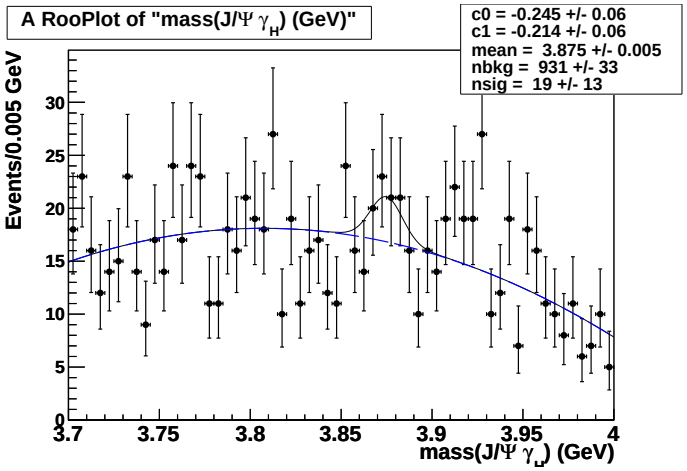

Figure 22: A Fit to the $m(J/\psi\gamma) - m(l^+l^-) + m(J/\psi)$ mass distribution for the sum of data samples at $\sqrt{s} = 4.230$ GeV and $\sqrt{s} = 4.260$ GeV.

Because there is no signal observed in the $\sqrt{s} = 4.360$ GeV data sample, the data samples of $\sqrt{s} = 4.230$ GeV and $\sqrt{s} = 4.260$ GeV are added together as shown in Figure 22 and the significance is calculated to be 1.61 σ.

4.6 Background Estimation

For the background estimation the 500 pb^{-1} inclusive MC sample generated at $\sqrt{s} = 4.260$ GeV mentioned before is used. It consists of all possible background contributions listed in Table 4 and 5. These samples are used check which background passes the final selection criteria as described in section 4.4, and the remaining background events of the inclusive MC sample are listed in Table 8. In total 3365 events pass the final selection criteria.

decay chain	nEvt	iTopo
$\psi(4260) \to \pi^0 J/\psi,\ J/\psi \to \mu^-\mu^+$	937	11
$\psi(4260) \to \gamma\chi_{c2},\ \chi_{c2} \to \gamma J/\psi,\ J/\psi \to \mu^-\mu^+$	698	2
$\psi(4260) \to \pi^0 J/\psi,\ J/\psi \to e^-e^+$	483	10
$\psi(4260) \to \gamma\chi_{c1},\ \chi_{c1} \to \gamma J/\psi,\ J/\psi \to \mu^-\mu^+$	391	1
$\psi(4260) \to \gamma\chi_{c2},\ \chi_{c2} \to \gamma J/\psi,\ J/\psi \to e^-e^+$	331	3
$\psi(4260) \to \gamma\chi_{c1},\ \chi_{c1} \to \gamma J/\psi,\ J/\psi \to e^-e^+$	229	0
$\psi(4260) \to \eta' J/\psi,\ \eta' \to \gamma\gamma,\ J/\psi \to \mu^-\mu^+$	89	12
$\psi(4260) \to \pi^0\pi^0 J/\psi,\ J/\psi \to \mu^-\mu^+$	72	15
$\psi(4260) \to \eta' J/\psi,\ \eta' \to \gamma\gamma,\ J/\psi \to e^-e^+$	46	14
$\psi(4260) \to \pi^0\pi^0 J/\psi,\ J/\psi \to e^-e^+$	31	13
$\psi(4260) \to \eta J/\psi,\ \eta \to \gamma\gamma,\ J/\psi \to \mu^-\mu^+$	7	16
$\psi(4260) \to \gamma\chi_{c0},\ \chi_{c0} \to \gamma J/\psi,\ J/\psi \to \mu^-\mu^+$	5	4
$\psi(4260) \to \gamma,\ \to \gamma J/\psi,\ J/\psi \to \mu^-\mu^+$	4	5
$\psi(4260) \to \eta J/\psi,\ \eta \to \gamma\gamma,\ J/\psi \to e^-e^+$	3	17
$\psi(4260) \to \gamma\chi_{c0},\ \chi_{c0} \to \gamma J/\psi,\ J/\psi \to e^-e^+$	2	8
$\psi(4260) \to \gamma\chi_{c2},\ \chi_{c2} \to \pi^-\rho^+,\ \rho^+ \to \pi^0\pi^+$	1	9
$\psi(4260) \to \gamma,\ \to \gamma J/\psi,\ J/\psi \to e^-e^+$	1	9
$\psi(4260) \to \gamma\chi_{c1},\ \chi_{c1} \to \gamma J/\psi,\ J/\psi \to e^-e^+\gamma$	1	6
$\psi(4260) \to \pi^0 J/\psi,\ J/\psi \to \pi^-\pi^+$	1	18
Radiative dimuon events	30	
Bhabha events	3	
Total number of inclusive background events	3365	

Table 8: Remaining background from inclusive MC sample at $\sqrt{s} = 4.260$ GeV, here iTopo refers to the topology ID given from the program for resonant background contributions.

The remaining contribution from **non-resonant background**, from QED are radiative dimuon and Bhabha events compared to Table 8, is shown in Figure 23. Here 30 dimuon events and three Bhabha events so in total only 33 events pass the selection criteria. Those possible background channels will contribute to a flat distribution in $M(\gamma J/\psi)$ invariant mass compared to the bottom plot in Figure 23, where no peak is formed from the background.

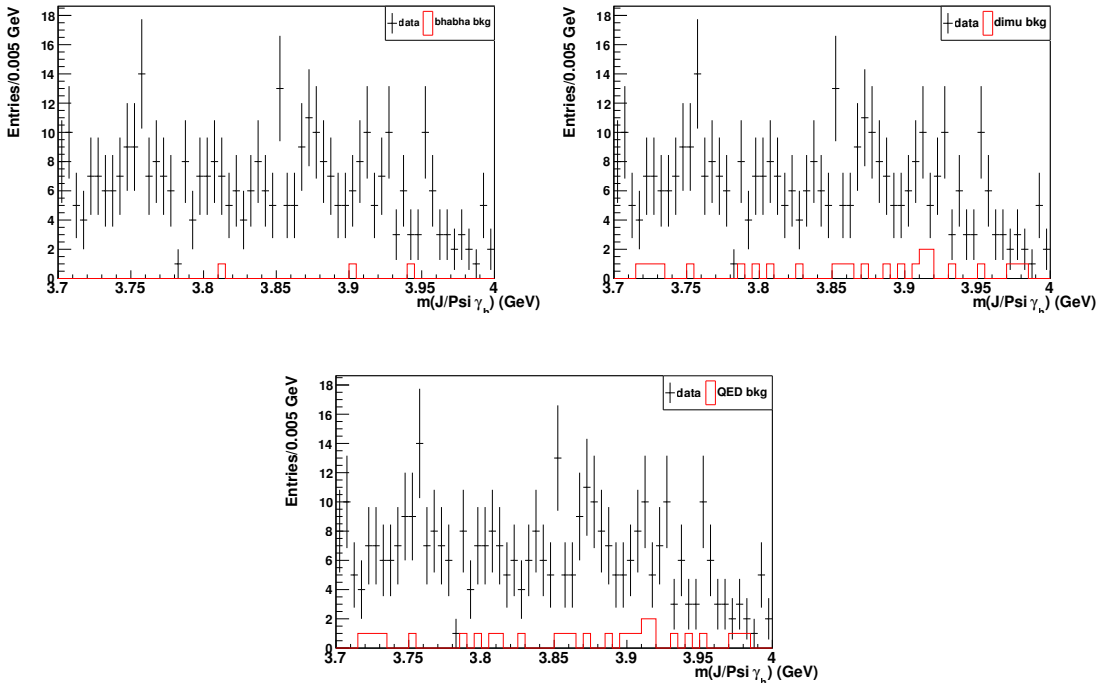

Figure 23: Non-resonant background contribution from QED production passing the final event selection compared to the data samples at $\sqrt{s} = 4.260$ GeV. In the top left picture remaining Bhabbha events and in top left the contirbution from dimuon events are shown. The bottom plot shows the sum of all remaining possible non-resonant background contributions.

The spectrum of the remaining **resonant background** is shown in Figure 24. Here the different topologies are shown in different color, where the topology ID corresponds to the ones given in Table 8 for the different background contributions. All those possible remaining backgrounds are drawn on top of each other (stacked), where the background events which are contributing the most are on the bottom of the distribution. This has the advantage that one can see the total spectrum of the remaining resonant background.

In Figure 25 all those remaining possible background contributions are shown compared to the invariant mass spectrum $M(\gamma J/\psi)$ of the data at $\sqrt{s} = 4.260$ GeV. The data and the resonant contribution are drawn normalized to compare their distribution in the same histogram, the QED contribution is not normalized since it would be to small to remain visible. From the comparison it can be seen that the QED contributions can be neglected because it will not form a peak in the $X(3872)$ mass region.

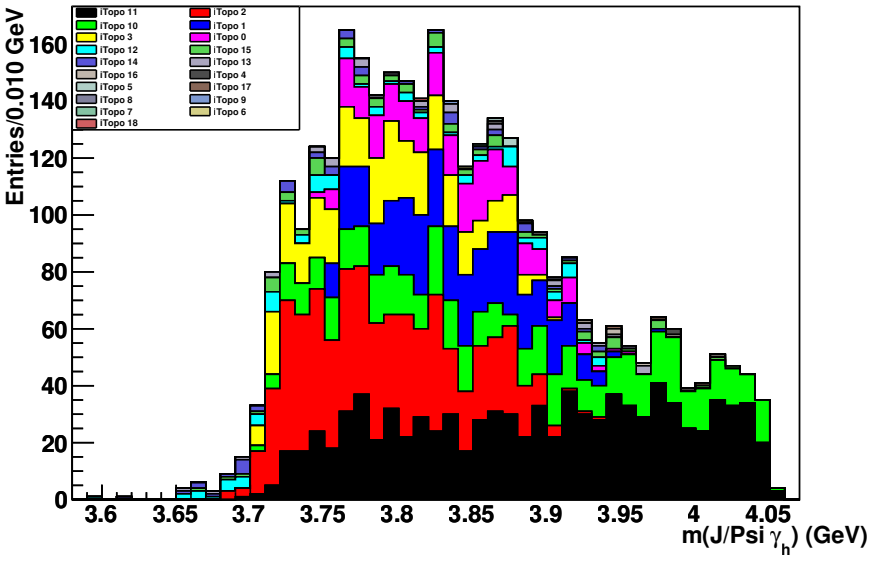

Figure 24: Resonant background contributions passing the final event selection. The different topologies can be distinguished due to their topology ID given in Table 8 and their corresponding different color as given in the legend.

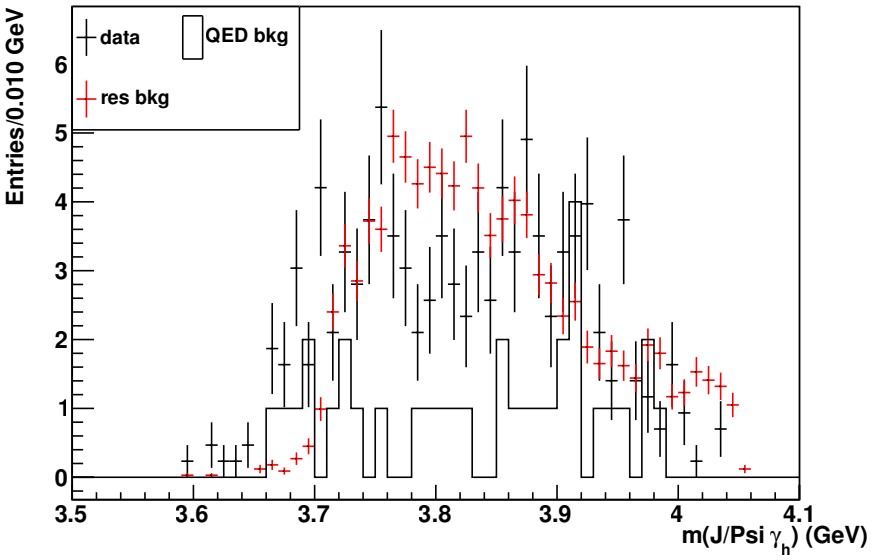

Figure 25: Comparison of the $M(\gamma J/\psi)$ invariant mass distribution from data taken at $\sqrt{s} = 4.260$ GeV (black errorbars) to remaining inclusive resonant background (red errorbars) and non-resonant (black lines) contribution.

If the resonant background contributions can be also neglected has to be further tested, since some of the possible remaining background contribute to the region around the $X(3872)$ mass. Those studies are done in the next section.

4.6.1 Resonant Background Estimations

The dominant background contributions are shown in Figure 26 not in the stacked form to see which background distribution really contribute in the region of the $X(3872)$ signal.

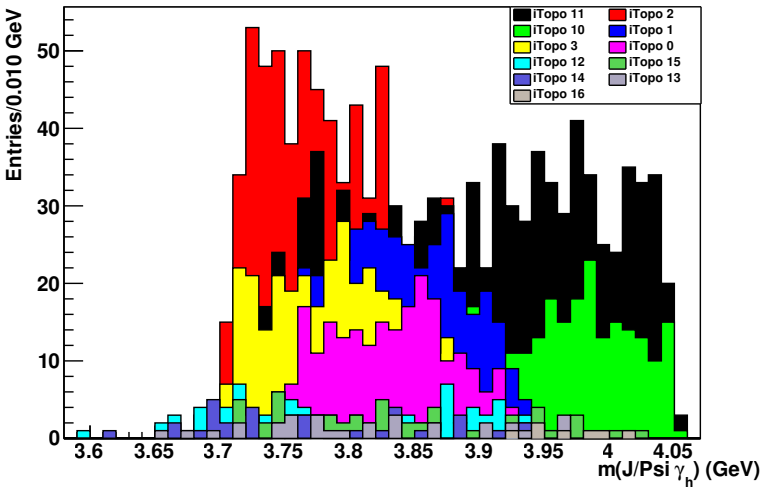

Figure 26: The dominant resonant background distributions and their possible contribution at the $X(3872)$ mass for inclusive MC samples at $\sqrt{s} = 4.260$ GeV.

Especially the ones with topology ID zero, one, two and eleven will contribute, these correspond to the background contribution of:

$$\psi(4260) \to \gamma\chi_{c1},\ \chi_{c1} \to \gamma J/\psi,\ J/\psi \to e^-e^+$$
$$\psi(4260) \to \gamma\chi_{c1},\ \chi_{c1} \to \gamma J/\psi,\ J/\psi \to \mu^-\mu^+$$
$$\psi(4260) \to \gamma\chi_{c2},\ \chi_{c2} \to \gamma J/\psi,\ J/\psi \to \mu^-\mu^+$$
$$\psi(4260) \to \pi^0 J/\psi,\ \pi^0 \to \gamma\gamma,\ J/\psi \to \mu^-\mu^+$$

One has to keep in mind that those are only *possible* background contributions, which does not mean that they really exist in data and form a peak.

Their contribution to data has to be checked by looking for possible χ_{c1} and χ_{c2} signals in the invariant mass of the lower energetic photon with the J/ψ signal in the data, which was done in Figure 27. No clear χ_{c1} and χ_{c2} signals can be observed in data which is in agreement with preliminary searches for $e^+e^- \to \gamma\chi_{cJ}$ at the different energy points presented in [55]. Only upper limits were presented in their analysis, since no significant signal was observed. Therefore this kind of background contribution can be neglected is this analysis.

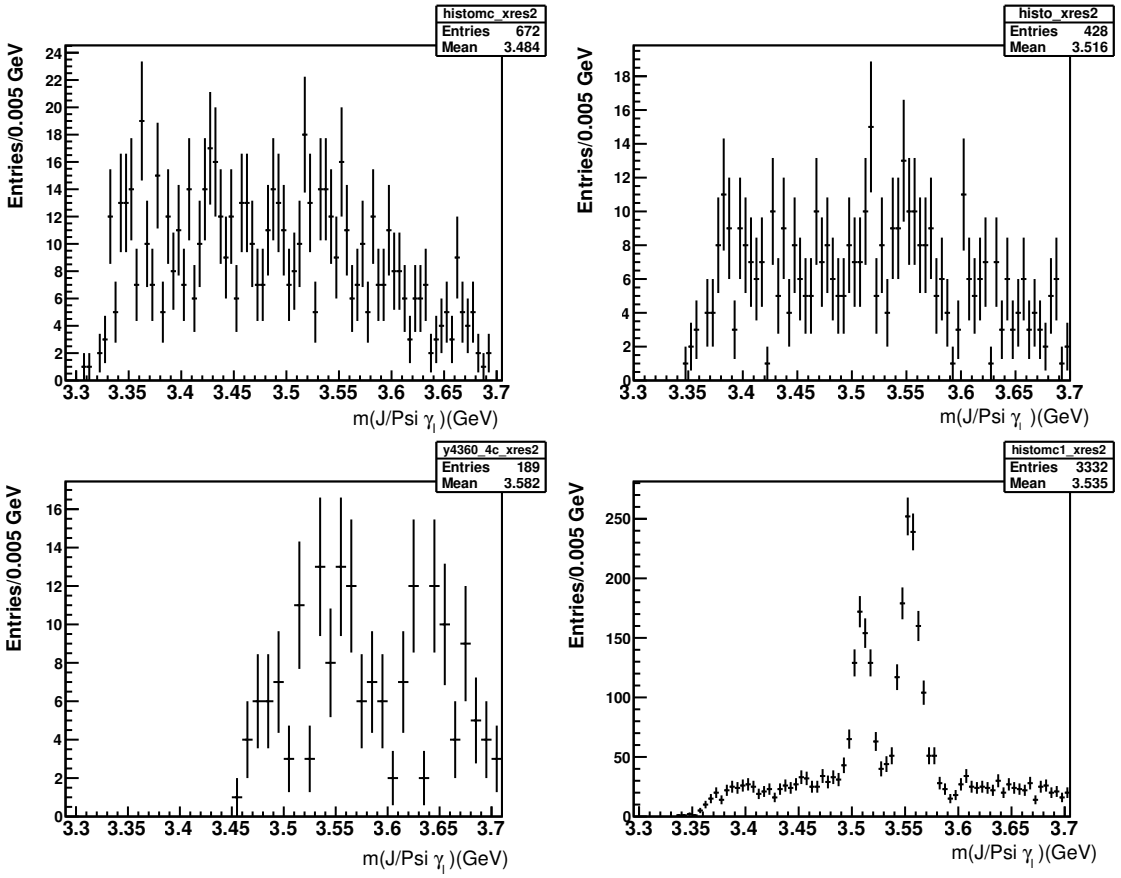

Figure 27: Check for χ_{c1} and χ_{c2} signals in the invariant mass $M(\gamma_l J/\psi)$ distribution in data samples taken at $\sqrt{s} = 4.230$ GeV (top left), $\sqrt{s} = 4.260$ GeV (top right) and $\sqrt{s} = 4.360$ (bottom left) GeV. The χ_{c1} and χ_{c2} signals from resonant inclusive MC which pass the final selection criteria are shown for comparison in the bottom right plot.

Possible contributions from $\psi(4260) \to \pi^0 J/\psi,\ J/\psi \to \mu^-\mu^+, e^+e^-$ can be estimated by looking for π^0 signals in the invariant mass of $m(\gamma\gamma)$. This spectrum is shown in Figure 28 for the different data sets and the π^0 signal from inclusive MC simulation on the bottom right after the final selection criteria, which includes an η-veto. Here no π^0 signal can be observed in the different data samples so that this background contribution can also be neglected.
This kind of background should be suppressed, since the final state has due to the pion an isospin of one. Because the strong interaction conserves isospin and if the initial state is a pure $c\bar{c}$ state with isospin zero, this decay would be an isospin violating decay which is rare in the charmonium system compared to the PDG [2].

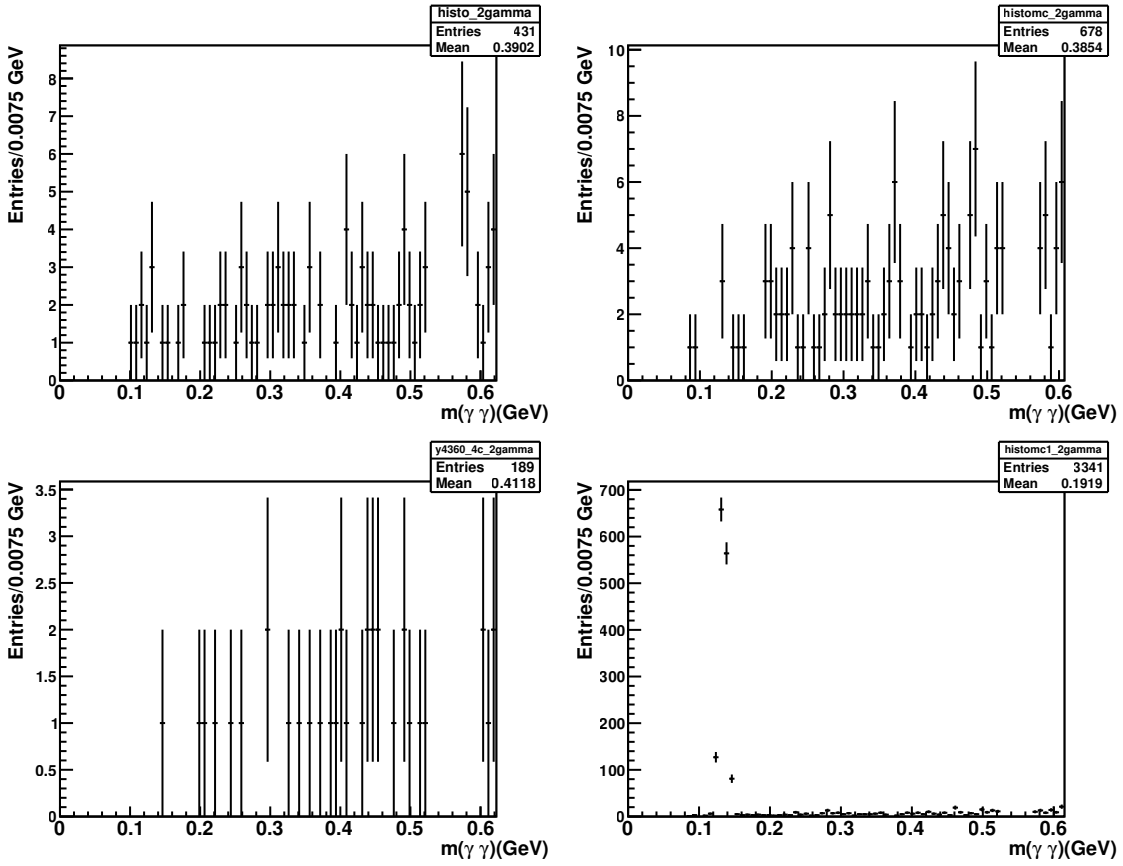

Figure 28: The distribution of $m(\gamma\gamma)$ invariant mass after all cuts for data samples taken at $\sqrt{s} = 4.230$ GeV (top left), $\sqrt{s} = 4.260$ GeV (top right) and $\sqrt{s} = 4.360$ (bottom left) GeV. The π^0 signal from resonant inclusive MC, which pass the final cuts, is shown for comparison in the bottom right plot.

Remaining background contributions from $\psi(4260) \to \eta J/\psi,\ J/\psi \to \mu^-\mu^+, e^+e^-$ are suppressed by the η- veto used in the final selection criteria compared to Figure 14 in section 4.4. Therefore only ten of those events remain from the inclusive MC samples, their contribution in data can be neglected.

Background contributions from $\psi(4260) \to \eta' J/\psi,\ J/\psi \to \mu^-\mu^+, e^+e^-$ also pass the final selection compared to Table 8, this can be estimated by looking for η' signals in $m(\gamma\gamma)$. This distribution can be seen in Figure 29 for data and inclusive MC background. In the data no η' signal is observed therefore this background contribution can also be neglected.

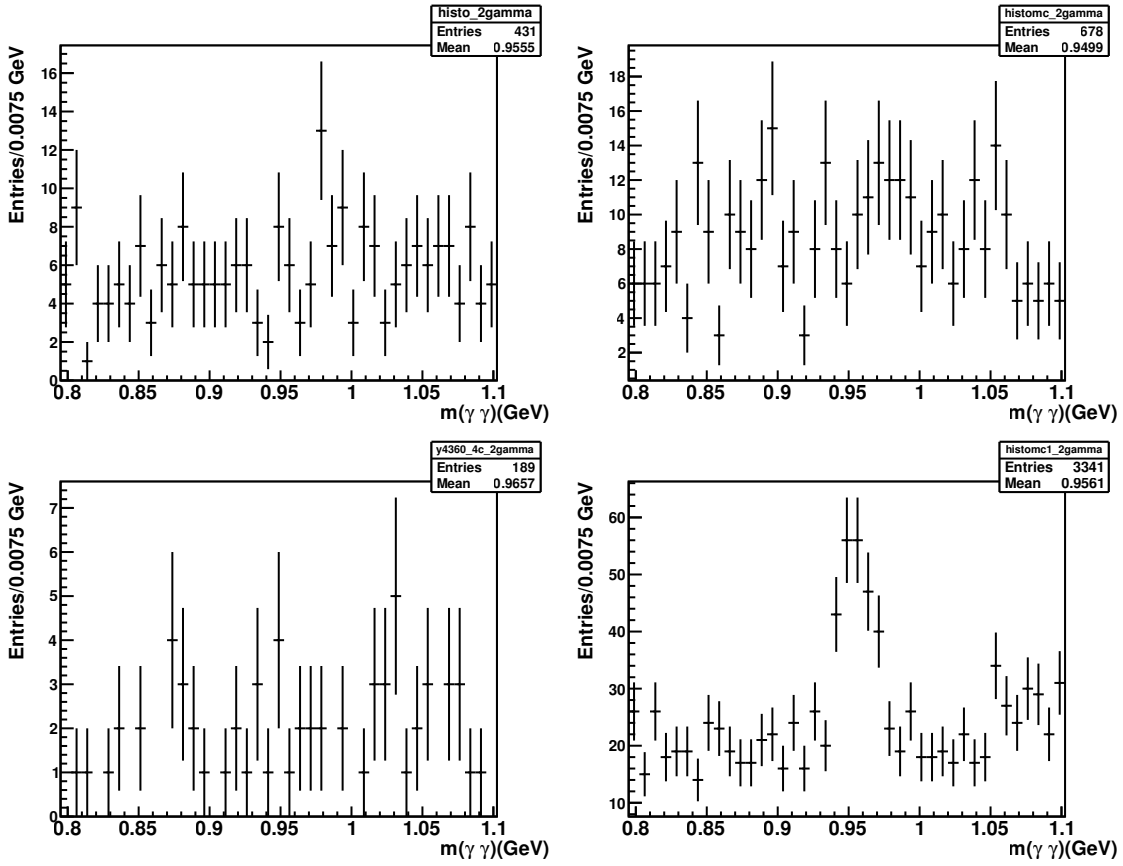

Figure 29: The distribution of $m(\gamma\gamma)$ invariant mass after all cuts for data samples taken at $\sqrt{s} = 4.230$ GeV (top left), $\sqrt{s} = 4.260$ GeV (top right) and $\sqrt{s} = 4.360$ (bottom left) GeV for the η' mass region. The η' signal from resonant inclusive MC, which pass the final selection criteria, is shown in the bottom right plot for comparison.

The background contribution can also be estimated by the side band of $X(3872)$ signal events. Those side bands are defined as the region, which are 5-8σ away from the J/ψ peak observed in data with $3.000 < m(l^+l^-) < 3.058$ GeV and $3.1403 < m(l^+l^-) < 3.20$ GeV. Those events are then combined with the higher energetic photon to the $M(\gamma J/\psi)$ invariant mass. The comparison of signal and side band events are shown in Figure 30. In the region of the $X(3872)$ mass, the signal events in the sum of all data events show a peak whereas the side band has a flat contribution.

A test for the performance of the used final selection criteria is done by studying the influence of the cuts onto a produced phase space MC simulation of $\gamma\gamma J/\psi$ without an included resonance. In total 100000 events are simulated. The distribution of events passing those selection criteria is shown in left of Figure 31 for the $X(3872)$ signal region, it is fitted with a phase space function which describes the events very well. Important is that no peak is created from the current selection criteria. The normalized distribution (drawn in green) compared to signal (drawn in black) and side band events (drawn in red) from data is shown on the right of Figure 31 for comparison.

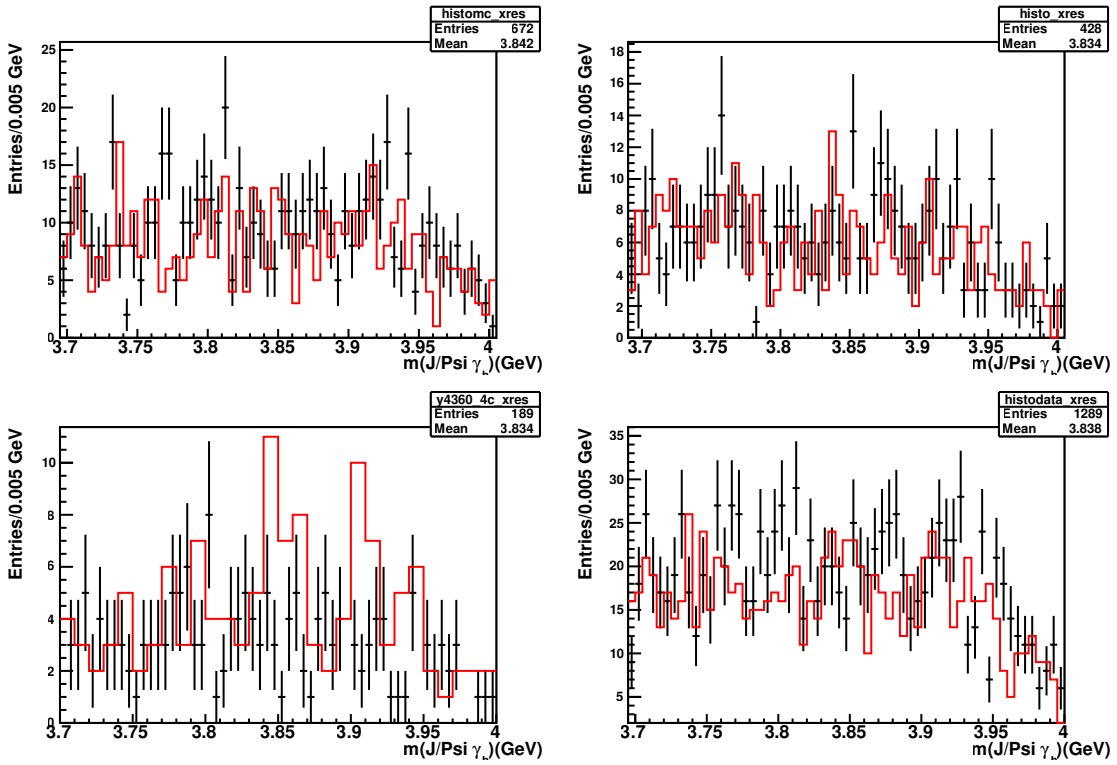

Figure 30: The distribution of $M(\gamma J/\psi)$ invariant mass after all cuts for signal events (drawn in black) versus side band events (drawn in red) for data taken at $\sqrt{s} = 4.230$ GeV (top left), $\sqrt{s} = 4.260$ GeV (top right), $\sqrt{s} = 4.360$ GeV (bottom left) and the sum of all data samples(bottom right).

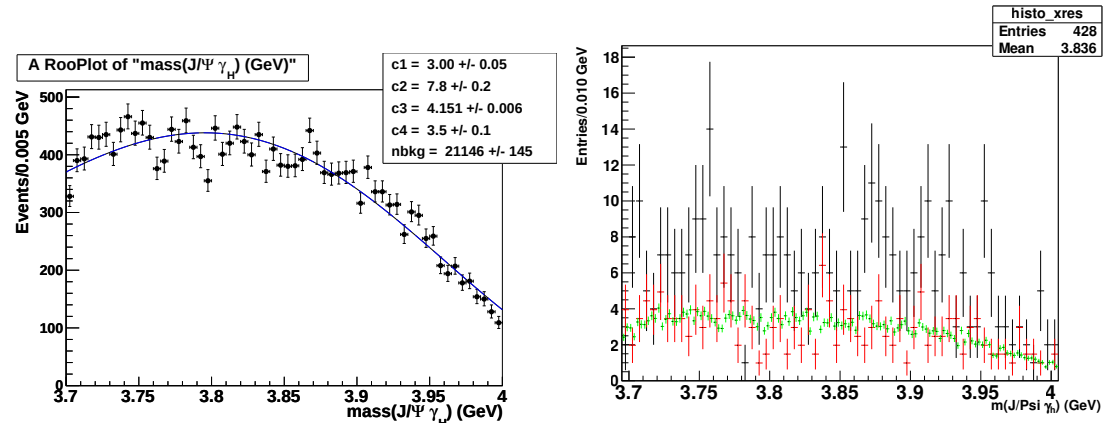

Figure 31: The distribution of $M(\gamma J/\psi)$ invariant mass invariant mass after the final selection criteria for simulated phase space events fitted with a phase space function (left) and the simulated phase space events (green) in comparison to signal events drawn in black and side band events drawn in red for data taken at $\sqrt{s} = 4.260$ GeV (right).

With those studies on possible background contributions, which could explain the enhancement in the region around the $X(3872)$ mass, it can be concluded that no peaking background remains in the data.

4.7 Systematic Uncertainties

Some sources of systematic errors are calculated in this section, due to the limited time of the thesis it was not possible to do a full analysis of systematic errors. Those have to be taken into account for the calculation of the upper limit for the cross section measurements of the different data sets done in the next section.

4.7.1 Uncertainty from luminosity measurement

The integrated luminosities for the data sets at $\sqrt{s} = 4.230$, 4.260 and 4.360 GeV have been measured using Bhabha events ($e^+e^- \to (\gamma)e^+e^-$) and as a cross check also digamma events ($e^+e^- \to \gamma\gamma$) in [56]. Their results are given in Table 9. To be conservative they state a total systematic error of 1% for each luminosity at the different data sets.

$\sqrt{s}$(GeV)	Luminosity (pb^{-1})
4.229	1091.74 $\pm$0.15 $\pm$ 10.92
4.260	825.67 $\pm$0.13 $\pm$ 8.26
4.360	539.84 $\pm$ 0.10 $\pm$ 5.40

Table 9: Measured luminosities and their uncertainties of data samples used in this analysis taken from [56]

4.7.2 Tracking Uncertainties

The uncertainty of the MDC tracking efficiency for high momentum leptons is 1% per track, that gives in total a systematic error of 2% for the uncertainty of tracking.

4.7.3 Uncertainties of Photon Selection

The systematic error due to photon detection uncertainties is obtained to be less than 1% per photon in a well understood channel of $J/\psi \to \rho\pi^0$ with $\rho \to \pi^+\pi^-$ and $\pi^0 \to \gamma\gamma$ by the data quality group in [57]. Therefore the systematic uncertainty for the selection of the two photons of the final state $l^+l^-\gamma\gamma$ is calculated to be 2 % in total.

4.7.4 Uncertainty concerning the Fitting Range

The uncertainty due to the fitting range is estimated by changes of the signal yield in fitting the invariant mass $m(J/\psi\gamma)$ as a final state with a $X(3872)$ resonance in data at $\sqrt{s} = 4.260$ GeV with a fitting range of 3.8 to 3.95 GeV as used in [1] instead of the previously used range of 3.7 to 4.0 GeV. From the cross section change due

to the new upper limit on the signal yield the systematic uncertainty is calculated to be 4.5 %.

4.7.5 Uncertainty of Background Shape

In the fit to obtain the $X(3872)$ signal yield, a first order Chebyshev function is used to describe the background. When using a second order Chebyshev function as a background shape the number of signals changes and leads to 4.9% difference in the cross section measurement, which is taken as the systematic error of background shape.

4.7.6 Uncertainty of Signal Shape

The $X(3872)$ signal in the data is fitted with fixed resonance parameters obtained from MC simulations at $\sqrt{s} = 4.260$ GeV by fitting the MC signal with a Breit-Wigner convolved with a Gaussian function. To get the uncertainty of the signal shape, the data is fitted with the direct MC signal shape simulated with KKMC assuming the $e^+e^- \to \gamma X(3872)$ events are produced via $Y(4260)$ decays. The difference in signal yield gives a cross section uncertainty of 0.4%, which is taken as the systematic error from signal parametrization.

4.7.7 Uncertainties from $Y(4260)$ line-shape

The $Y(4260)$ line-shape will affect the radiative correction factor $(1 + \delta)$ and the detection efficiency. Using the measurements from BESIII, Belle and *BABAR* [10, 11, 58] as an input, the maximal difference in $(1 + \delta) \cdot \epsilon$ was calculated in [1] to be 0.6%. This value is taken as the systematic error from line-shape measurements.

4.7.8 Uncertainties of branching ratios

The branching ratio measurement of $J/\psi \to l^+l^-$ is taken from [2]. The systematic error is 1% for $J/\psi \to l^+l^-$.

4.7.9 Total systematic uncertainties

Table 10 summarizes all systematic errors sources and their contributions which were calculated. The total systematic error is calculated by adding all errors in quadrature, assuming all sources are independent of each other. This gives a total systematic error of 7.4 %.

Source	Error (%)
Luminosity	1.0
Tracking Efficiency	2.0
Photon Selection	2.0
Fitting Range	4.5
Background Shape	4.9
Signal Shape	0.4
$Y(4260)$ line-shape	0.6
branching ratio	1.0
Total	7.4

Table 10: Summary of systematic errors for cross section estimation.

4.8 Upper limits on cross sections

The statistical significance calculated in section 4.5 is smaller than 5 σ. Thus no observation of the $X(3872)$ has been made and an upper limit has to be calculated. For the fits performed to calculate the signal significance in section 4.5 the central value and the number of signal events are floating parameters, only the signal shape was fixed from fits to MC simulations. The central value fits for calculating the upper limit is set to the range obtained from those previously done fits.

The calculation of upper limits is done using the Bayesian method, where a fit to the invariant mass spectrum is performed fixing the number of signal events N_i to a value from ranging from zero to 50. Here steps of 0.1 are used and for each step a fit is performed with the corresponding fixed number of events and the likelihood is calculated. These likelihoods are divided by the total maximum likelihood obtained by a fit of floating number of signal events and then plotted against the number of signal events. With this the upper limit for the number of signals is determined by finding the value of number of signal events (N_i) corresponding to 90% of the likelihood distribution by integrating the area of the function up to 90%. These upper limits for the decay modes $e^+e^- \to \gamma X(3872)$, $X(3872) \to \gamma J/\psi(e^+e^-, \mu^+\mu^-)$ at 90% confidence level (C.L.) are given in Table 11 and the corresponding likelihood functions are shown in Figure 32, where the upper limit of signal events is indicated by an arrow.

$\sqrt{s}$(GeV)	upper limit of N_i
4.229	20.4
4.260	26.7
4.360	10

Table 11: Upper limits for the number of signal events for different data sets at 90 % C.L.

With these numbers the upper limit for the cross section can be calculated. The

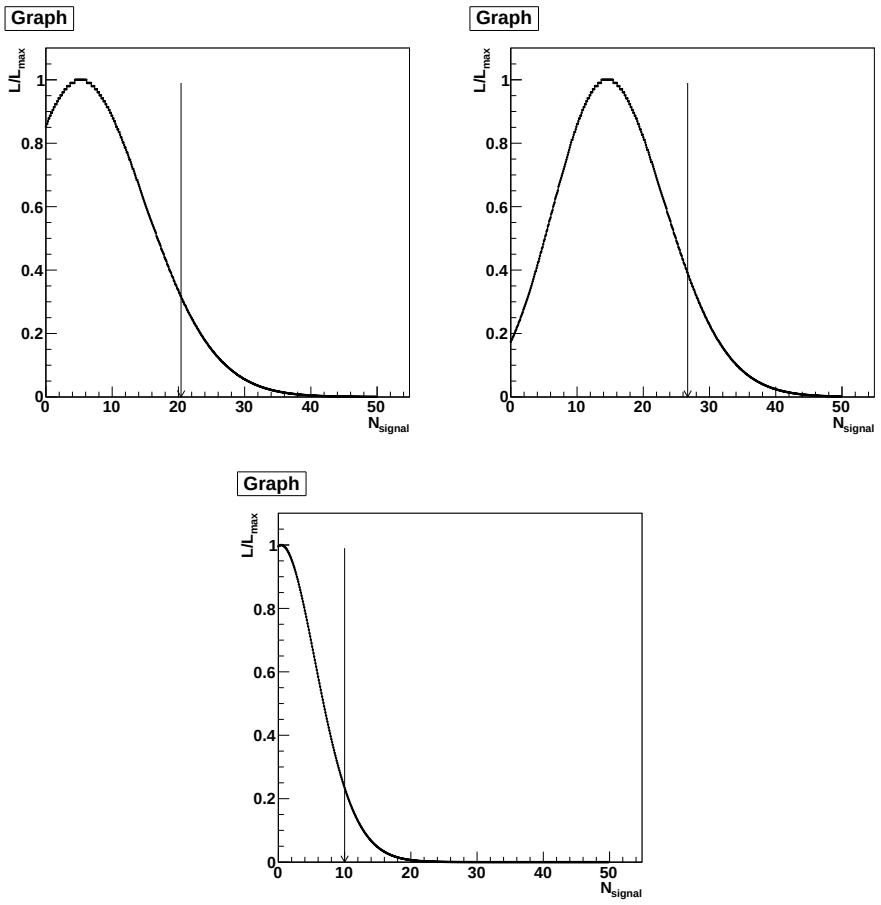

Figure 32: Likelihood values normalized to the maximal likelihood versus the fitted number of possible $X(3872)$ events calculated for steps of 0.1 signal events at $\sqrt{s} = 4230$ MeV (top left), $\sqrt{s} = 4260$ MeV (top right) and $\sqrt{s} = 4360$ MeV (bottom).

$\sqrt{s}$(GeV)	N^{obs}	N^{up}	$\epsilon(\%)$	$\mathcal{L}_{int}(pb^{-1})$	$(1+\delta)$	$\sigma^B \cdot \mathcal{B}$(pb)
4.229	5.3 ± 9.8	< 20.4	34.4	1094	0.799	< 0.617
4.260	14.5 ± 8.3	< 26.7	34.0	827	0.814	< 1.061
4.360	0.4 ± 5.3	< 10.0	33.1	545	1.023	< 0.493

Table 12: Upper limits at 90 % C.L. for the cross section measurements at different energy points.

Born cross section formula is given by

$$\sigma^B = \frac{N_{signal}}{\mathcal{L}_{int}(1+\delta)\epsilon\mathcal{B}} \tag{6}$$

where N_{signal} is the upper limit on number of signal events which was calculated before and $\mathcal{L}_{int}$ is the integrated luminosity for each data sample given in Table 3. ϵ is the final selection efficiency calculated from signal MC given in Table 6, $\mathcal{B}$ is the branching fraction of $J/\psi \to l^+l^-$ which is taken from the PDG [2] to be $11.87 \pm 0.085\%$. $(1+\delta)$ is the radiative correction factor , which is defined as

$$(1+\delta) = \frac{\sigma^{obs}}{\sigma^B} = \frac{\int \sigma^B(s(1-x))F(x,s)dx}{\sigma^B(s)}. \tag{7}$$

Here $F(x,s)$ is the radiator function which is calculated from QED with an accuracy of 0.1%. $\sigma^B(s)$ is the Born cross section shape of the $e^+e^- \to \gamma X(3872)$ production process. Because a higher cross section is observed at $\sqrt{s} = 4.23$ GeV and 4.26 GeV the assumption is that the $e^+e^- \to \gamma X(3872)$ cross section shape follows the $Y(4260) \to J/\psi\pi^+\pi^-$ line shape. Therefore the measured $Y(4260)$ line shape parameters from published results [10, 11, 58] can be used as input parameters for KKMC. The corresponding output values are taken from [1] to be 0.799, 0.814 and 1.023 at $\sqrt{s} = 4.23$ GeV, 4.26 GeV and 4.26 GeV respectively. Those calculated values are in good agreement with QED calculations from [59].

Using the upper limits on the number of signal events in Table 11 the upper limit for the measured Born cross section for $e^+e^- \to \gamma X(3872)$ times the branching ratio $\mathcal{B}(X(3872) \to J/\psi\gamma)$ can be calculated to be

$$\sigma^B[e^+e^- \to \gamma X(3872)] \cdot \mathcal{B}(X(3872) \to J/\psi\gamma) \begin{cases} < 0.617 \text{ pb at } \sqrt{s} = 4.23 \text{ GeV} \\ < 1.061 \text{ pb at } \sqrt{s} = 4.26 \text{ GeV} \\ < 0.493 \text{ pb at } \sqrt{s} = 4.36 \text{ GeV} \end{cases}$$

where the efficiency has been lowered by the factor $(1 - \sigma_{syst})$, with σ_{syst} is the systematic uncertainty calculated in the previous chapter to be 7.4%.

Together with all used values for the calculation, the upper limits for the cross sections are summarized in Table 12.

5 Summary and Conclusions

A search for the radiative decays of $Y(4260)/Y(4360) \to \gamma X(3872)$ with the subsequent decay of $X(3872) \to \gamma J/\psi$ for data collected with the BESIII experiment directly taken at these resonances was performed. From previous measurements at different experiments about seven events were expected since the efficiency from MC is estimated to be comparable. With the current statistics 18.4 ± 13.5 events were observed in the total sum of all data what is in agreement with the expected number of events, but the statistical significance is only 1.59 σ. This means that those possible signal events could also be a statistical fluctuation with no real signal events. More data taken at those energy points would help to really exclude or confirm the signal.
The significance was calculated from the maximum likelihood method by comparing the maximum likelihood values for fits of signal and background functions with fits describing the background only. This value can be related by Wilks theorem to the statistical significance.

Since the significance is smaller than 5σ, as shown in the first column of Table 13, which is the threshold to state an observation, upper limits for the signal cross sections were calculated:

$\sqrt{s}$(GeV)	signal significance	$\sigma_B[e^+e^- \to \gamma X(3872)] \cdot \mathcal{B}(X(3872) \to J/\psi\gamma)$(pb)
4.229	0.57	< 0.617 at 90% C.L.
4.260	2.12	< 1.061 at 90% C.L.
4.360	0.51	< 0.493 at 90% C.L.

Table 13: Upper limits at 90 % C.L. for the cross section measurements at different energy points.

The upper limits were calculated with the Bayesian method: performing a fit to the data and calculating the corresponding maximum likelihood for a fixed number of signal events. These likelihoods were plotted against the number of signal events. The area corresponding to 90 % of the total area under this likelihood curve determines the upper limit of signal events at 90% C.L..
The efficiency was lowered by the systematic uncertainty $\epsilon \cdot (1 - \sigma_{syst})$ which was calculated to be 7.4%.
Due to the limited extent of this thesis it was not possible to do a full analysis of the systematic errors, errors from cut efficiencies of selection cuts as well as the error for the kinematic fit efficiencies are missing. Those uncertainties need to be evaluated from a control channel with a clean data sample from efficiency differences in MC and data. The problem is that there is no proper channel at $\sqrt{s} = 4.260$ GeV with the same final state $J/\psi\gamma\gamma$ as analysed in this work. Therefore a new channel at a lower energy (e.g. $\psi(2S) \to J/\psi\eta$, $\eta \to \gamma\gamma$) would have to be studied and optimized from cut selections, which would be a new analysis and could not be done here.

Radiative transitions of $Y(4260)/Y(4360) \to \gamma X(3872)$ are important to understand

the exotic features of the involved states as well as to probe the commonality of those states. If the decay is confirmed it can have important implications for the structure of both states, then is seems very likely that their nature is the same as for example both being molecules [60]. With the current statistics the existence of this decay and the subsequent decay of $X(3872) \to \gamma J/\psi$ could not be observed. More data would be needed to confirm that the measured cross section can be described by the resonant contribution of the $Y(4260)$ line shape as investigated in [1]. Other $X(3872)$ final state decay channels such as into $\bar{D}^{*0}D^0$ or $\psi(2S)\gamma$, which still needs confirmation, look more promising to confirm the radiative transition.

6 Deutsche Zusammenfassung

Im Charmonium Spektrum wurden viele Zustände entdeckt, die nicht durch theoretische Modell vorhergesagt wurden und daher nicht in das Spektrum passen. Charmonia lassen sich theoretisch mithilfe von Potentialmodellen beschreiben. Eingesetzt in die nicht-relativistische Schrödinger-Gleichung können schon einfache Potentiale gute Vorhersagen des $c\bar{c}$ Massenspektrums liefern. Diese entdeckten Zustände können aufgrund ihrer Eigenschaften keine konventionell gebundenen $c\bar{c}$ Zustände sein und werden als QCD erlaubte exotische Zustände verstanden.
Einer dieser exotischen Zustände ist das $X(3872)$, welches schon 2003 durch die Belle Kollaboration entdeckt wurde, allerdings ist die zugrunde liegende Natur des Teilchens noch immer nicht bekannt, obwohl dessen Eigenschaften fast alle vermessen wurden. Auch wurden einige vektorartige Zustände ($Y(4260)$, $Y(4360)$) entdeckt, die bisher nicht verstanden sind.

Die vorliegende Arbeit beschäftigt sich mit der Suche nach dem Prozess $e^+e^- \to \gamma X(3872)$, wobei das $X(3872)$ durch $J/\psi\gamma$ rekonstruiert wird. Dabei wurden die Daten für diese Analyse am BESIII Detektor bei Schwerpunktsenergien an den exotischen Resonanzen $Y(4260)$ und $Y(4360)$ genommen, um diese Zustände hinsichtlich ihrer Art genauer untersuchen zu können. BESIII ist am symmetrischen e^+e^- Speichering BEPCII des IHEP Instituts in Peking, China in Betrieb und beschäftigt sich mit τ- und Charm Physik bei Schwerpunktsenergien bis zu 4.66 GeV.
In dieser Analyse wird insbesondere nach dem radiativen Übergang zwischen den zwei exotischen Zuständen $Y(4260)/Y(4360) \to \gamma X(3872)$ gesucht, um dessen Existenz zu überprüfen, da dieser schon durch BESIII [1] beobachtet wurde.

Die erwartete Anzahl von Ereignissen kann aus vorherigen Untersuchungen durch verschiedene Experimente zu sieben Ereignissen abgeschätzt werden. Die Analyse des gesamten Datensatzes ergab 18.4 ± 13.5 Signal Ereignisse. Dies ist vereinbar mit der Abschätzung, allerdings wurde mit den gegebenen Datenmengen nur eine statistische Signifikanz von 1.59 σ erreicht, was weit weg von einer Entdeckung bei 5 σ liegt. Um eine Aussage über die Existenz des Signals $e^+e^- \to \gamma X(3872)$ sowie $X(3872) \to J/\psi\gamma$ treffen zu können wird eine größere Datemenge für die entsprechenden Schwerpunktsenergien benötigt.
Daher wurde eine obere Grenze für das Produkt aus Signal Wirkungsquerschnitt und Verzweigungsverhältnis im 90% Konfidenzintervall für die verschiedenen Schwerpunktsenergien wie folgt bestimmt:

$$\sigma^B[e^+e^- \to \gamma X(3872)] \cdot \mathcal{B}(X(3872) \to J/\psi\gamma) \begin{cases} < 0.617 \text{ pb bei } \sqrt{s} = 4.23 \text{ GeV} \\ < 1.061 \text{ pb bei } \sqrt{s} = 4.26 \text{ GeV} \\ < 0.493 \text{ pb bei } \sqrt{s} = 4.36 \text{ GeV} \end{cases}$$

Dazu wurde die Effizienz aus MC Simulationen mit dem Faktor $(1 - \sigma_{syst})$ multipliziert, um die systematischen Fehler, die zu 7.4% berechnet wurden, mitberücksichtigen zu können.
Die obere Grenze der Signal Ereignisse wurde dabei mit der Methode nach Bayes

bestimmt. Dazu wurden die Daten mit einer festen Anzahl von Signal-Ereignissen gefittet, die maximale Wahrscheinlichkeit bestimmt und dann die Signal Anzahl variiert. Diese Wahrscheinlichkeiten wurden gegen die Signal Ereignisse aufgetragen und die Gesamtfläche unter der Verteilung bestimmt. Ein Konfidenzintervall von 90% entspricht dabei einer eingeschlossenen Fläche von 90%, welche die untere Grenze der Anzahl von Signal Ereignissen entspricht.

Mit der vorliegenden Analyse kann keine Aussage darüber getroffen werden, ob die Messung des Wirkungsquerschnittes durch eine $Y(4260)$-Resonanz besser beschrieben wird, als durch Kontinuums-Produktion, um damit den radiativen Zerfall aus [1] zu bestätigen. Andere $X(3872)$ Zerfallskanäle mit höheren Verzweigungsverhältnissen, wie zum Beispiel in $\bar{D}^{*0}D^0$ oder $\psi(2S)\gamma$, könnten erfolgversprechender für diese Bestätigung sein.

Die Untersuchung von radiativen Übergängen $Y(4260)/Y(4360) \to \gamma X(3872)$ ist wichtig für das Veständnis der Struktur dieser exotischen Zustände. Ein Nachweiß dieser Übergange würde für eine ähnliche exotische Struktur dieser Zustände und damit für eine Verbindung dieser sprechen. Diese Aussage wäre hilfreich für die theoretische Beschreibungen solcher Zustände, aber auch für das generelle Verständnis von nicht-pertubativer QCD.

List of Figures

List of Tables

References

[1] M. Ablikim et al. (BESIII Collaboration), Phys. Rev. Lett. **112**, 092001 (2014).

[2] J. Beringer et al. (Particle Data Group), Phys. Rev. D **86**, 010001 (2012).

[3] G. Aad et al., Physics Letters B **716**, 1 (2012).

[4] S. Chatrchyan et al., Physics Letters B **716**, 30 (2012).

[5] D. Griffiths, Introduction to Elementary Particles, Physics textbook (Wiley, 2008).

[6] E. Eichten et al., Phys. Rev. D **17**, 3090 (1978).

[7] J. Eiglsperger (2007), `hep-ph/0707.1269`.

[8] M. G. Ullrich, Ph.D. thesis, Justus-Liebig-Universität Gießen (2013).

[9] T. Barnes et al., Phys. Rev. **D72**, 054026 (2005).

[10] M. Ablikim et al. (BESIII Collaboration), Phys. Rev. Lett. **110**, 252001 (2013).

[11] Z. Q. Liu et al. (Belle Collaboration), Phys. Rev. Lett. **110**, 252002 (2013).

[12] T. Xiao et al., Physics Letters B **727**, 366 (2013), ISSN 0370-2693.

[13] M. Ablikim et al. (BESIII Collaboration), Phys. Rev. Lett. **111**, 242001 (2013).

[14] R. Mizuk et al. (Belle Collaboration), Phys. Rev. D **78**, 072004 (2008).

[15] S.-K. Choi et al. (Belle Collaboration), Phys. Rev. Lett. **100**, 142001 (2008).

[16] M. Ablikim et al. (BESIII Collaboration) (2013), `hep-ex/1308.2760`.

[17] M. Ablikim et al. (BESIII Collaboration), Phys. Rev. Lett. **112**, 022001 (2014).

[18] S. Choi et al. (Belle Collaboration), Phys. Rev. Lett. **91**, 262001 (2003).

[19] D. Acosta et al. (CDF Collaboration), Phys. Rev. Lett. **93**, 072001 (2004).

[20] V. Abazov et al. (D0 Collaboration), Phys. Rev. Lett. **93**, 162002 (2004).

[21] B. Aubert et al. (BaBar Collaboration), Phys. Rev. **D71**, 071103 (2005).

[22] N. Brambilla et al., Eur. Phys. J. **C71**, 1534 (2011).

[23] A. Abulencia et al. (CDF Collaboration), Phys. Rev. Lett. **98**, 132002 (2007).

[24] B. Aubert et al. (BaBar Collaboration), Phys. Rev. **D74**, 071101 (2006).

[25] V. Bhardwaj et al. (Belle Collaboration), Phys. Rev. Lett. **107**, 091803 (2011).

[26] R. Aaij et al. (LHCb), Phys. Rev. Lett. **110**, 222001 (2013).

[27] B. Aubert et al. (BaBar Collaboration), Phys. Rev. **D77**, 011102 (2008).

[28] T. Aushev et al. (Belle Collaboration), Phys. Rev. **D81**, 031103 (2010).

[29] K. Abe et al. (Belle Collaboration) (2005), `hep-ex/0505037`.

[30] P. del Amo Sanchez et al. (BaBar Collaboration), Phys. Rev. **D82**, 011101 (2010).

[31] B. Aubert et al. (BaBar Collaboration), Phys. Rev. Lett. **102**, 132001 (2009).

[32] B. Aubert et al. (BaBar Collaboration), Phys. Rev. Lett. **96**, 052002 (2006).

[33] X. Liu (2013), `hep-ph/1312.7408`.

[34] W. Chen et al. (2013), `hep-ph/1311.3763`.

[35] B. Aubert et al. (BaBar Collaboration) (2008), `hep-ex/0808.1543`.

[36] C. Z. Yuan et al. (Belle Collaboration), Phys. Rev. Lett. **99**, 182004 (2007).

[37] Q. He et al. (CLEO Collaboration), Phys. Rev. D **74**, 091104 (2006).

[38] B. Aubert et al. (BABAR Collaboration), Phys. Rev. Lett. **98**, 212001 (2007).

[39] X. L. Wang et al. (Belle Collaboration), Phys. Rev. Lett. **99**, 142002 (2007).

[40] T. E. Coan et al. (CLEO Collaboration), Phys. Rev. Lett. **96**, 162003 (2006).

[41] S. Lange (2013), `hep-ex/1311.7594`.

[42] M. Ablikim et al., Nuclear Instruments and Methods in Physics Research Section A: Accelerators, Spectrometers, Detectors and Associated Equipment **614**, 345 (2010).

[43] D. Asner et al., Int. J. Mod. Phys. **A24**, S1 (2009).

[44] Z. Chuan et al., Chinese Physics C **35**, 72 (2011).

[45] C. Liu, Journal of Physics: Conference Series **293** (2011).

[46] W.-D. Li et al., Int. J. Mod. Phys. **A24**, 9 (2009).

[47] URL `http://bes3.ihep.ac.cn/system/offline/offline.htm`.

[48] S. Agostinelli et al., Nuclear Instruments and Methods in Physics Research Section A: Accelerators, Spectrometers, Detectors and Associated Equipment **506**, 250 (2003).

[49] F.-K. Guo et al., Physics Letters B **725**, 127 (2013).

[50] B. Aubert et al. (BaBar Collaboration), Phys. Rev. **D77**, 111101 (2008).

[51] S. Jadach et al., Comput. Phys. Commun. **130**, 260 (2000), `hep-ph/9912214`.

[52] A. Ryd et al. (2005).

[53] Z. Deng et al., Chinese Phys. C **30**, 371 (2006).

[54] S. S. Wilks, Ann. Math. Statist. **9**, 60 (1938).

[55] Z. He et al. (2014), URL `http://hnbes3.ihep.ac.cn/HyperNews/get/AUX/2014/03/15/13.32-90551-gamma_chicj_memo_v3.pdf`.

[56] Q. Gao et al. (2013), URL `http://hnbes3.ihep.ac.cn/HyperNews/get/AUX/2013/12/22/08.28-5845-luminosity.pdf`.

[57] M. Ablikim et al. (BESIII Collaboration), Phys. Rev. D **83**, 112005 (2011).

[58] J. P. Lees et al. (BABAR Collaboration), Phys. Rev. D **86**, 051102 (2012).

[59] E. Kuraev and V. Fadin, Sov. J. Nucl. Phys. **41**, 466 (1985).

[60] E. Swanson (2014), `hep-ph/1401.3914`.

Acknowledgements

First of all I would like to thank Prof. Dr. Wolfgang Kühn for giving me the opportunity to do my Thesis in his working group and be part of his group in general with a nice working atmosphere. It was a great pleasure for me to work in the international BESIII collaboration as well as to work on such an interesting and up-to-date topic. I am really thankful that I got the opportunity to work at the experiment and do shifts in China. I had a really nice time working on this topic and I learned a lot during this time.
I would like express my thanks Dr. Sören Lange for his support and long helpful discussions on general subjects like statistic and fitting tools concerning this thesis. Without the help and the encouragement of Hua Ye many parts of the thesis would be missing. Thanks a lot for fruitful discussions, your time to talk about my results and the help to connect with people in the collaboration.
Matthias Ullrich also helped me a lot on how to do a proper analyses and on coding. I would like to thank also the rest of the working group, especially Milan and Björn, for good discussions, help with the BOSS software and C++ as well as a nice working environment.
I am much obliged to Marcel Werner for proofreading my thesis, thank you very much for being patient with me and answering me all my questions especially in the final time of the thesis. I will miss the time with you as an office mate and friend, especially because of your nice distractions.
A big thanks goes to my parents for their parental support during the whole time of the thesis, I am so grateful that they helped me so much that I could really focus only on to my thesis.
Last but not least I would like to thank my boyfriend Niklas for his encouragement and his great support during that time. I don't know what I would have done without you, thank you always believe in me and your motivation.

Eidesstattliche Versicherung

Ich erkläre hiermit an Eides statt, dass ich die vorliegende Arbeit selbstständig und ohne Benutzung anderer als der angegebenen Hilfsmittel angefertigt und wissenschaftlich erarbeitet habe; die aus fremden Quellen direkt oder indirekt übernommenen Gedanken sind als solche kenntlich gemacht. Bei den von mir durchgeführten Untersuchungen habe ich die Grundsätze guter wissenschaftlicher Praxis, wie sie in der "Satzung der Justus-Liebig-Universität Gießen zur Sicherung guter wissenschaftlicher Praxis" niedergelegt sind, eingehalten.
Die Arbeit wurde bisher in keiner Form einer anderen Prüfungskommission vorgelegt oder veröffentlicht.

Gießen, den 31. März 2014

Svende Annelies Braun